NASA CR-121244

SELF-HEALING FUSE DEVELOPMENT

by

N. D. Jones, R. E. Kinsinger and L. P. Harris

GENERAL ELECTRIC COMPANY

prepared for

NATIONAL AERONAUTICS AND SPACE ADMINISTRATION

NASA Lewis Research Center
Contract NAS3-14388
G. R. Sundberg, Project Manager

I

FINAL REPORT

SELF-HEALING FUSE DEVELOPMENT

by

N. D. Jones, R. E. Kinsinger and L. P. Harris

GENERAL ELECTRIC COMPANY
Tube Products Department
Microwave Tube Operation
Schenectady, New York

prepared for

NATIONAL AERONAUTICS AND SPACE ADMINISTRATION

January 30, 1973

CONTRACT NAS3-14388

I

FOREWORD

The work described herein was performed by the General Electric Microwave Tube Operation under NASA Contract NAS3-14388 with N. D. Jones as the principal investigator. G. R. Sundberg, NASA-Lewis Research Center was Project Manager.

TABLE OF CONTENTS

ABSTRACT

The mercury-filled self-healing fuses developed for this program afford very good protection from circuit faults with rapid reclosure. Fuse performance and design parameters have been characterized. Life tests indicate a capability of 500 fuse operations. Fuse ratings are 150 volts at 5, 15, 25 and 50 circuit amperes. A series of sample fuses using alumina and beryllia insulation have been furnished to NASA for circuit evaluation.

SUMMARY

The purpose of this program was to design, fabricate, test and evaluate mercury-filled self-healing fuses. The nominal fuse ratings were 5, 15, 25 and 50 amperes at 150 dc circuit volts. Fuses should tolerate 600 volt surges and be capable of 1000 or more operations.

Earlier work on these devices had shown that the fuse action occurs in three stages: (1) an energy limiting stage defined by the energy required to heat the liquid mercury to its boiling temperature, causing the channel to fill with mercury vapor and break down to a mercury arc discharge; (2) a transition stage where voltage rises rapidly to a high peak value while current decays and explosive forces expel all liquid mercury from the fuse channel; (3) an arc stage when the mercury arc persists for times of the order of 10^{-5} to 10^{-2} second with an arc impedance 100 or more times greater than the resistance of the liquid mercury column.

Two factors are important to the selection of materials and designs for these devices: (1) the device must withstand the explosive transition forces and (2) the fuse channel materials must withstand a very large flux of heat energy dissipated while the fuse arc persists. Alumina and beryllia ceramics were selected as fuse channel materials for this work. External metal rings were designed to pre-compress the ceramics, thus preventing the ceramic from being damaged by the explosive transition forces. Fuses using channel diameters ranging from 0.15 to 1.2 mm were fabricated and tested. Larger channel fuses had only one channel, while the smaller channel devices had up to twelve. The smaller diameter channels using extruded ceramic tubing molded in glass presented formidable problems in fuse fabrication. However, the larger channel devices are machined from solid alumina and fewer fabrication problems are encountered. Fuses of both designs have been furnished to NASA for further evaluation.

A simple bellows, heavily spring-loaded and mechanically restrained to resist impact forces, adequately provides the elastic characteristics required of the fuse container. These devices are sealed off by means of a novel technique utilizing silicone rubber.

A fuse test station with an SCR-switched test circuit was designed and fabricated for testing these devices. Fuse tests under a variety of simulated fault conditions can be accomplished with this versatile circuit.

A standardized set of test procedures was established to evaluate and compare the performance of the various fuses tested. Three major fuse characteristics were evaluated: circuit protective capability, fuse arc extinction and impedance, and fuse channel erosion.

This program has provided a better understanding of the extinction characteristics and the impedance of confined metal-vapor arcs through a combination of theoretical analysis and experimental evaluation. Good agreement was obtained between analysis and test data. Results show that faster switching action and higher arc impedance are characteristic of smaller diameter fuse channels. This characteristic high arc impedance coupled with the fast-switching capability of the self-healing fuse provide excellent circuit protection. In addition these factors will permit the use of lighter auxiliary switching devices in the protected circuit.

The explosive mechanical forces created during fuse operation were contained by structures embodying all-ceramic insulators, pre-stressed by force-fitted external metal rings. Fuses with a simpler ceramic configuration molded in glass were less durable. Life tests indicate capability of 500 operations when the fuse channel experiences 5 kW/cm^2 energy for 1 millisecond or less.

Fuse design parameters are described in relation to fuse cold resistance, fault current limiting action, arc extinction and arc impedance.

INTRODUCTION

The purpose of this program was to develop, design, fabricate, test and evaluate mercury-filled self-healing fuses. These devices interrupt an electric current under overload conditions and then automatically reestablish the conduction path within a time of the order of a millisecond. The general form of the fuse is a mercury-filled, closed container consisting of two end reservoirs electrically insulated but connected by a small channel. When excessive current flows through the channel, mercury is vaporized and the current is interrupted. The mercury conduction path is then restored by gravity-independent forces supplied by the container.

The nominal fuse ratings sought were 5, 15, 25 and 50 amperes at 150 nominal d-c circuit volts. Fuses should tolerate 600 volt surges and be capable of 1000 or more operations without failure. The fuse is to be storable between $-65^\circ C$ and $+150^\circ C$ and operable at ambient temperatures from $-30^\circ C$ to $+80^\circ C$. This report describes the work performed toward achieving these objectives.

This program is an extension of earlier work performed under NASA contract NAS12-675 and described in report NASA CR-72868. Background also was provided by prior art which has been documented.[*]

The self-healing fuse takes advantage of the large increase in electrical resistivity going from the liquid state to the gaseous vapor state for liquid metals. Thus, these devices have also been termed "Change of State Current Limiters". The operation of these fuses can be described in three stages: (1) The energy-limiting stage is defined by the energy required to heat the liquid mercury in the channel to its boiling temperature. The channel cross-section is then filled very rapidly by a bubble of neutral mercury vapor, which simultaneously breaks down to a mercury arc discharge. (2) In the transition stage, the fuse voltage initially rises very rapidly to a value determined by the circuit parameters, while current simultaneously decays at a rate determined by these parameters. During the transition stage explosive forces expel all the liquid mercury from the channel. (3) After the transition, the mercury arc either extinguishes or persists for times of the order of milliseconds with an arc impedance of 100 or more times greater than the resistance of the liquid mercury column.

---

[*] L. J. Golberg, patent No. 3,273,018; R. L. Hurtle, patent Nos. 3,117,203 and 3,158,786; L. P. Harris, patent No. 3,389,359; J. J. Keenan, patent No. 3,389,360

The explosive transition forces per unit area are high -- generating pressures of the order of 10,000 psi -- although the resulting net force is quite small due to the very small channel size. Similarly, the current limiting arc results in a large flux of heat energy per unit area for the fuse channel walls, although the circuit energy is limited to very modest levels by the high arc impedance. Since the transition occurs in a very short time and most of the transition energy becomes heat at the walls of the fuse channel, transition stage heat energy also becomes an important factor.

FUSE DESIGNS, MATERIALS AND FABRICATION TECHNIQUES

In terms of technology, the background available from the earlier work cited in the "Introduction" had established the existence of two major factors as governing the usefulness of these devices: (1) the device must mechanically withstand the explosive transition forces, and (2) the fuse materials must withstand the large flux of heat energy generated within the fuse channel during the transition explosion and any subsequent current-limiting arc action. Thus these two factors become primary considerations in selection of materials and designs for these devices. Because some practicable limits had to be established relative to the variations of materials and designs that could be evaluated, and since the availability and fabrication techniques favored the use of alumina or beryllia as an insulator, these two materials were established as the major candidates.

GLASS-MOLDED ALUMINA OR BERYLLIA DEVICES

Because analytical studies of the high-pressure metal vapor plasma had indicated some advantage for fuse channels with diameters of 0.2 mm or less (refer to Appendix A), work effort during the early phases of this program were directed to small diameter, multi-channel devices. These devices utilized commercially available two- and seven-hole 99 percent pure alumina and two-hole beryllia tubing.

The tubing was molded in glass having a coefficient of expansion similar to alumina and beryllia. Two design variations of these glass-molded fuses are shown in cross-section in Figures 1 and 2. The external rings in each design are nickel alloy with a thermal expansion slightly higher than glass or ceramic. Thus, the metal rings pre-compress the glass and ceramic as the assembly cools down after molding the glass in place. This pre-compression prevents the ceramic from being fractured by the tensile stresses induced by the explosive transition forces.

Several devices were fabricated using these fuse designs, but performance was inconsistent. X-ray examination showed that small voids (bubbles) had formed in the glass during the molding process, causing fractures in the glass and ceramic tubing. Mercury was filling the voids thus creating some electrical shorting of the fuse channels.

Fewer voids occurred in fuses of the glass-molded design shown in Figure 3; however, these voids were less likely to cause electrical shorting
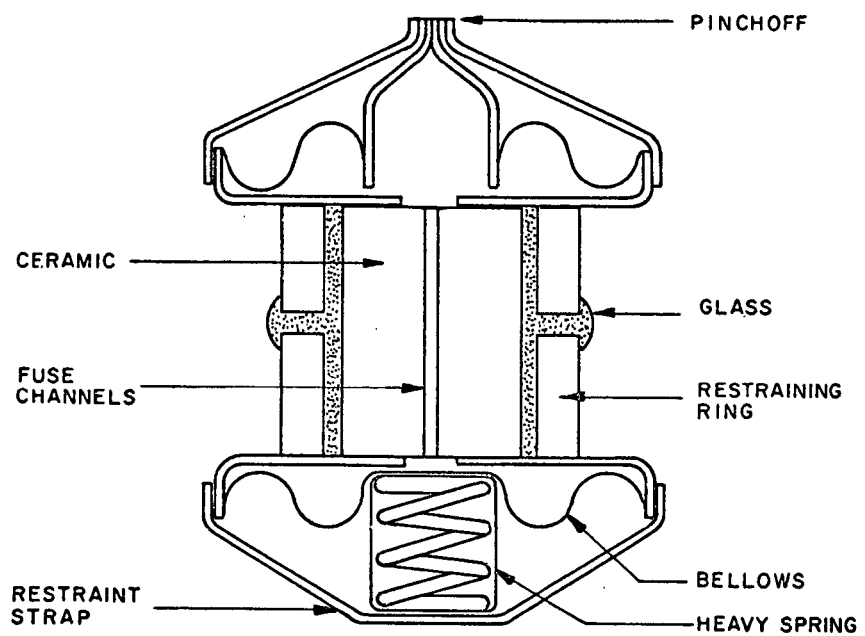
Figure 1 - Glass-Molded Fuse Design

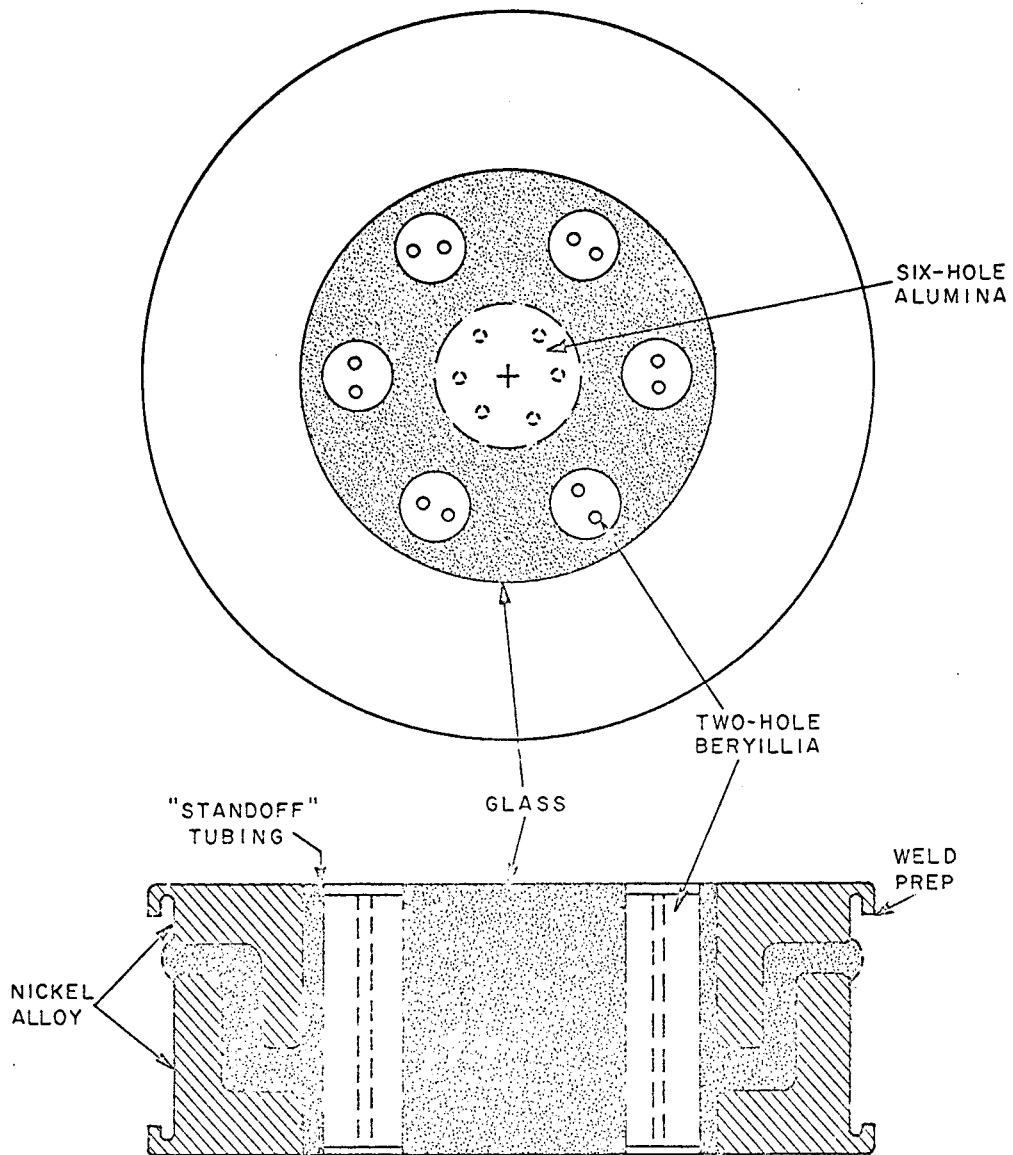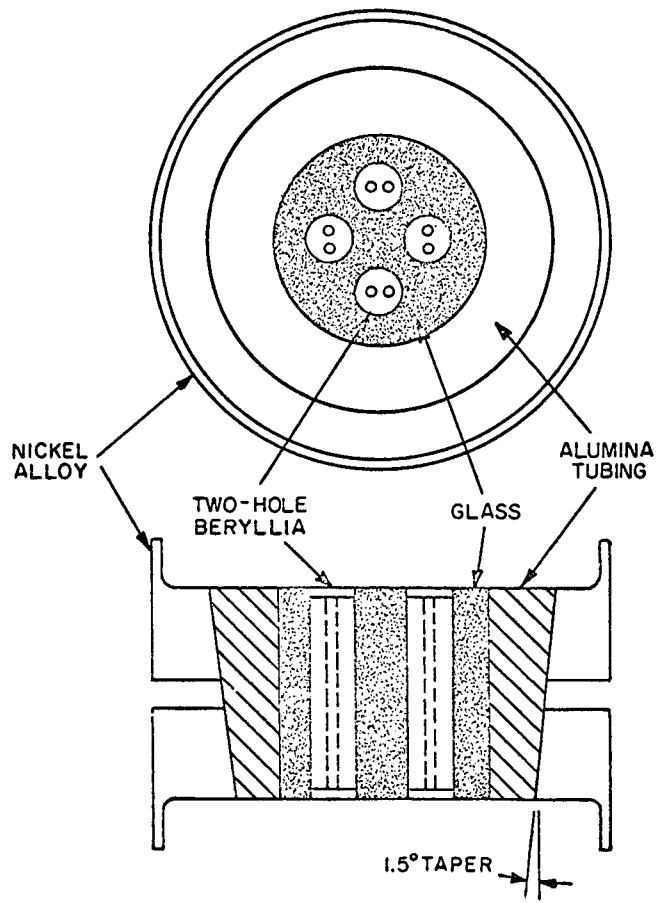Figure 2 - Glass-Molded Fuse Configuration

SIX-HOLE
ALUMINA

TWO-HOLE
BERYILLIA

"STANDOFF"
TUBING

GLASS

WELD
PREP

NICKEL
ALLOY

Figure 3 - Glass-Molded Tapered Fuse Design

Labels in figure: NICKEL ALLOY, TWO-HOLE BERYLLIA, GLASS, ALUMINA TUBING, 1.5° TAPER

because the alumina tubing utilized in this design served to insulate the external metal rings. Performance of these devices generally was superior to those of the Figures 1 and 2 design.

The pre-compression of the glass-molded assembly is achieved by forcing accurately fitted metal rings over the machine-tapered exterior of the alumina tubing. The design stresses the metal to its yield strength and the thermal expansions of metal and ceramic are an approximate match over the operating range.

The glass-molding technique used was relatively simple. Fuse parts were placed in a graphite fixture and heated in an air oven at 950 to 1000°C for approximately 10 minutes. Moderate pressure was applied by a weight or spring to force the glass into the fuse structure. Since the glass was always under compression and not subject to stress failure, heat treatment for reducing stresses was unnecessary.

A more critical fabrication technique was to prevent glass from filling holes in the inner ceramic tubing. Graphite rods or copper wires were placed in the ends of holes having a diameter larger than 0.3 mm. These were readily removed after the excess glass was machined off. Oversize graphite rods were forced into the holes and later drilled out. Copper wires slightly smaller than the holes were cemented in place with a slurry of isobutyl methacrylate binder and boron nitride powder and later the copper was etched out with hot aqua regia. The boron nitride strongly inhibits glass from entering the holes.

Smaller holes (0.15 to 0.3 mm in diameter) could be kept open with the copper wire technique, but graphite rods that small were unobtainable. A graphite cap was placed over each end of the small alumina tubing which extended beyond the outer alumina tubing. After the glass molding process was completed, the excess length of small tubing was machined off. Because of the toxicity of beryllia, machining could not be performed in the MTO shop, and as a result only the copper wire technique could be applied to the small beryllia tubing.

FUSE DESIGNS WITH ALL-CERAMIC INSULATORS

In order to fabricate fuses completely free of the voids experienced with glass-molded fuse assemblies, ceramic insulators with one, two and twelve small holes were fabricated of "ultra-pure" (99.9 percent) alumina body* prepared in General Electric's Microwave Tube Operation (MTO) Ceramic Laboratory.

* GE Proprietary

9

The design of the 1- or 2-hole devices is shown in Figure 4, and the fuse parts are shown pictorially in Figure 5. The pre-compression of the tapered ceramic member is provided by forcing three accurately fitted metal rings over the ceramic, as described for the glass-molded design of Figure 3. The use of three metal members allows narrower open spaces between rings and locates them near the ends of the fuse channel. This places the areas of sudden stress change, which will occur in the space between rings, at a location of lesser internal stress as compared to the center of the fuse channel where internal stress is at a maximum. The three-ring design is more feasible for longer fuses with a 24-mm long ceramic member. However, the shorter designs (Figure 3) with a ceramic 10-mm long are mechanically less amenable to the three-ring design, but fortunately, internal stresses are reduced because of the shorter length and smaller hole diameter.

Components for the all-ceramic short fuse design are photographed in Figure 6. The tapered ceramic shown has twelve 0.17-mm diameter holes. This ceramic was a 99.9 percent pure alumina cast body* fabricated in MTO ceramic laboratory. Two sample runs were made, but both produced porous ceramic bodies. Since considerable process development would have been required to produce non-porous bodies, the approach was abandoned. One fuse was assembled and tested briefly, but no significant results were obtained.

EXTERNAL FUSE STRUCTURE

The mechanical requirements for the external fuse structure are not stringent and consequently cause little difficulty. (The large per unit forces generated in the fuse channel cause only small net forces due to the very small area of the channel.) The fuse structure, however, must supply gravity-independent restoring forces to inject mercury back into the fuse channel after the fuse fires, and must also allow for thermal expansion and contraction of the mercury. To accommodate these requirements, end buffer sections consisting of a rigid cup and a spring-loaded flexible diaphragm in a cup configuration, as shown in Figures 4, 5, and 6 were provided on each end of the fuse.

Three completed fuses showing the heavy spring structure can be seen in Figure 7. Only one spring was provided for the shorter fuses, which have a smaller volume of mercury and require less flexibility of the end buffers.

Because the transition forces are of short duration, the impact effects of the force are quite high, and the diaphragm structure will be distorted

END
VIEW

1 OR 2
FUSE
CHANNELS

TAPERED
CERAMIC

SECTION
A-A

TAPERED
METAL RINGS

FLEXIBLE
DIAGRAM

ARC-WELDED

RESTRAINT
STRAP

WASHER

HEAVY
SPRING

PINCHOFF
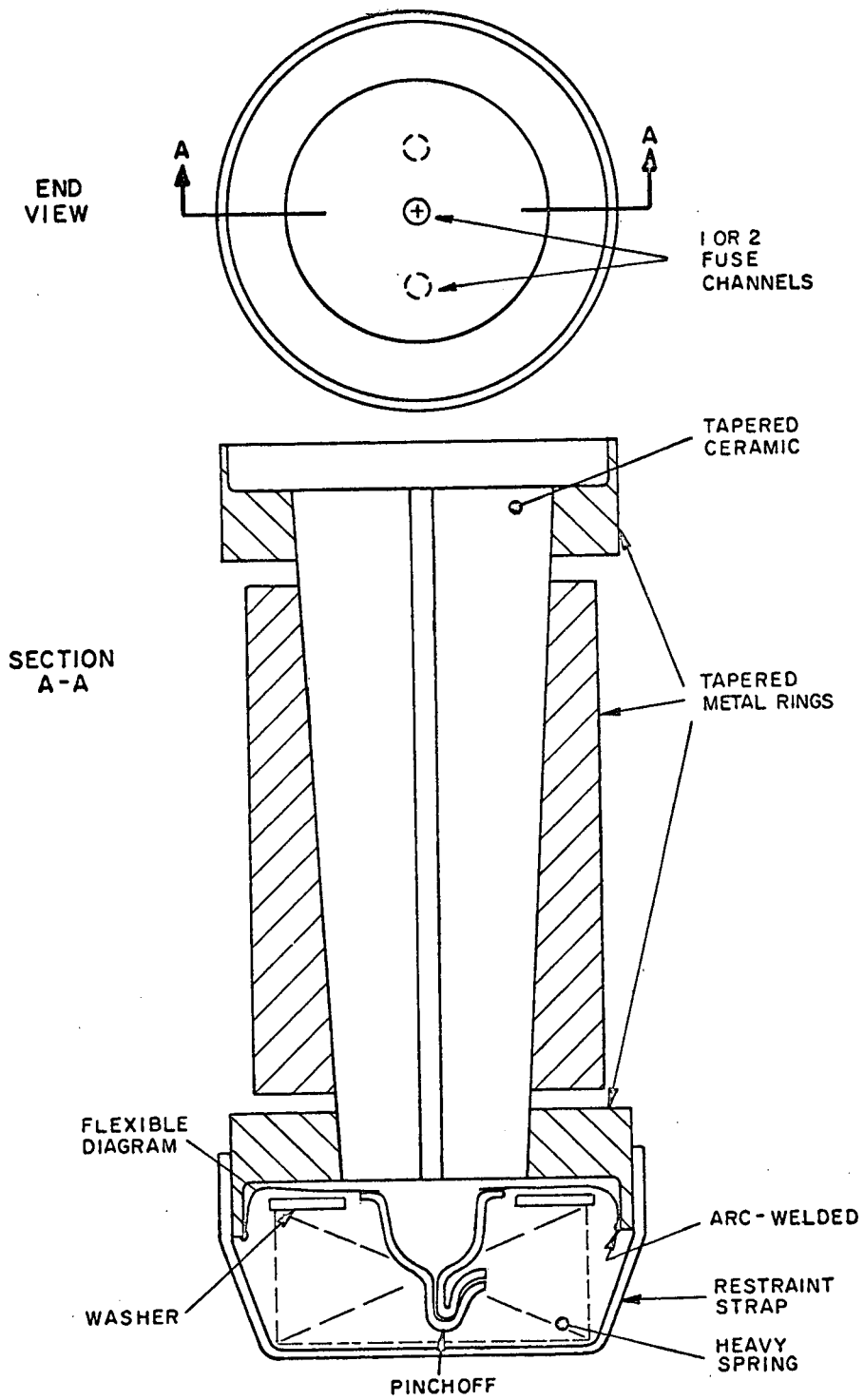
Figure 4 - Design for One- or Two-Channel Devices

11
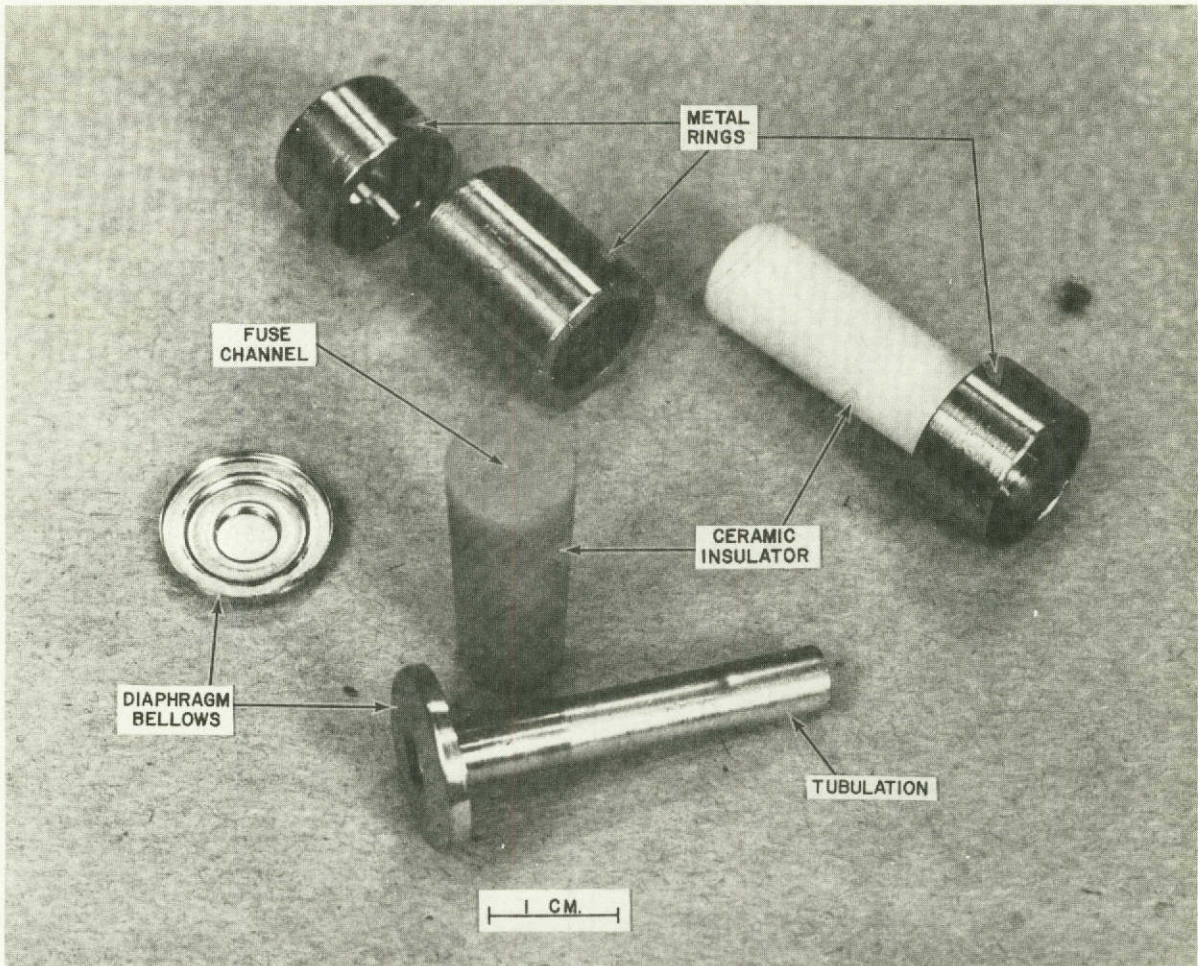
Figure 5 - Component Parts for One- or Two-Channel Devices
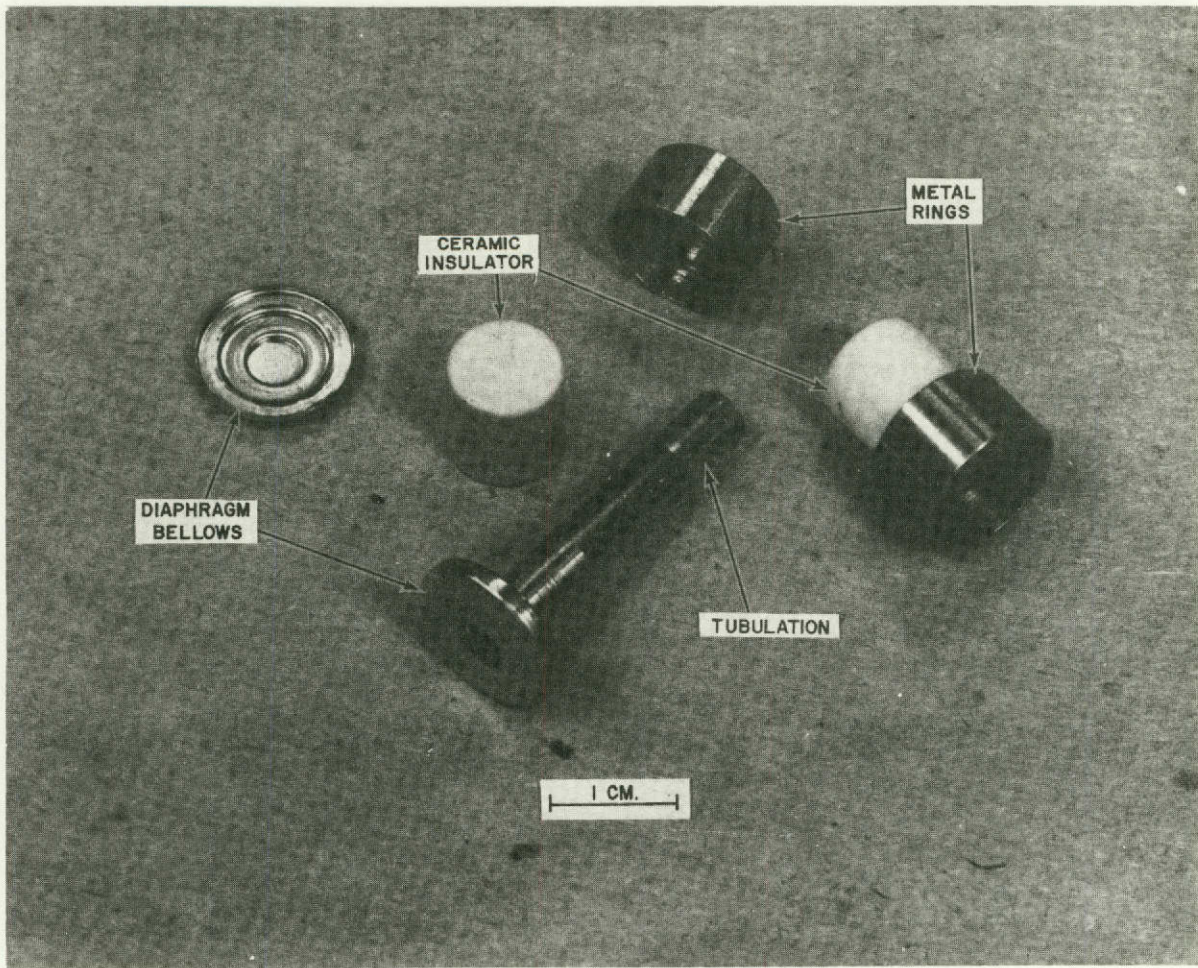
Figure 6 - Component Parts for All-Ceramic Short Fuses
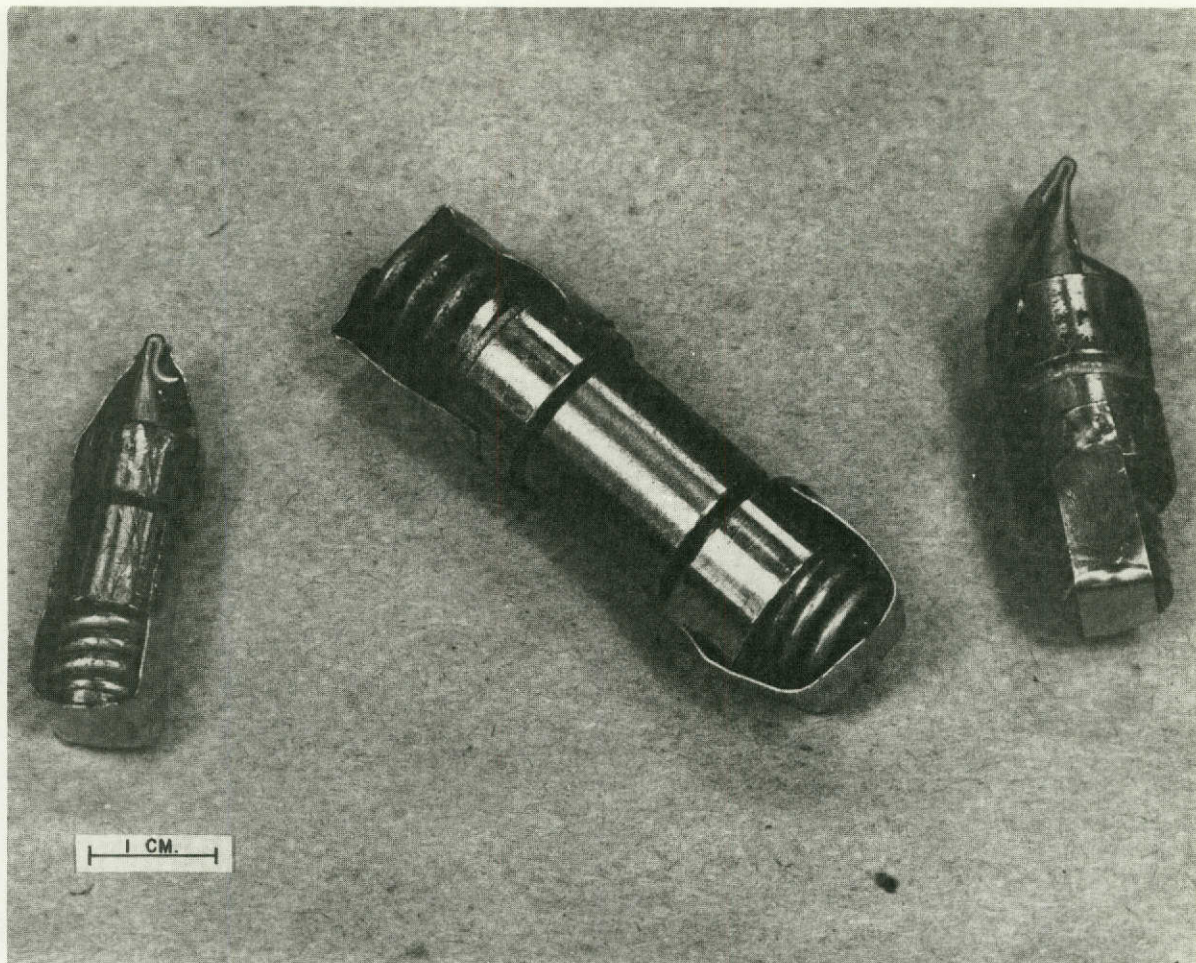
Figure 7 - Completed Fuses with Heavy Spring Structure

unless a strong restoring force is provided. This was accomplished by the heavy spring and a restraint strap which holds the spring almost fully compressed. The end buffer sections not only limit the impact-induced flexing of the diaphragm, but allow the diaphragm to move the required four percent (in volume) to provide for thermal expansion of the mercury.

A hermetic seal was provided for these fuses by a technique developed in earlier fuse work under NASA contract NAS12-675. This technique involves coating the interior of the tubulation with a thin layer of silicone rubber (shown at the left in Figure 8) during fuse fabrication. When the fuse is ready for sealing-off, the tubing is flattened and folded, as seen at the right in the figure, thus effecting a hermetic seal.

RUBBER
COATING

TUBING

FLATTENED
AND FOLDED
OVER

COATED
TUBULATION

AFTER
SEAL-OFF
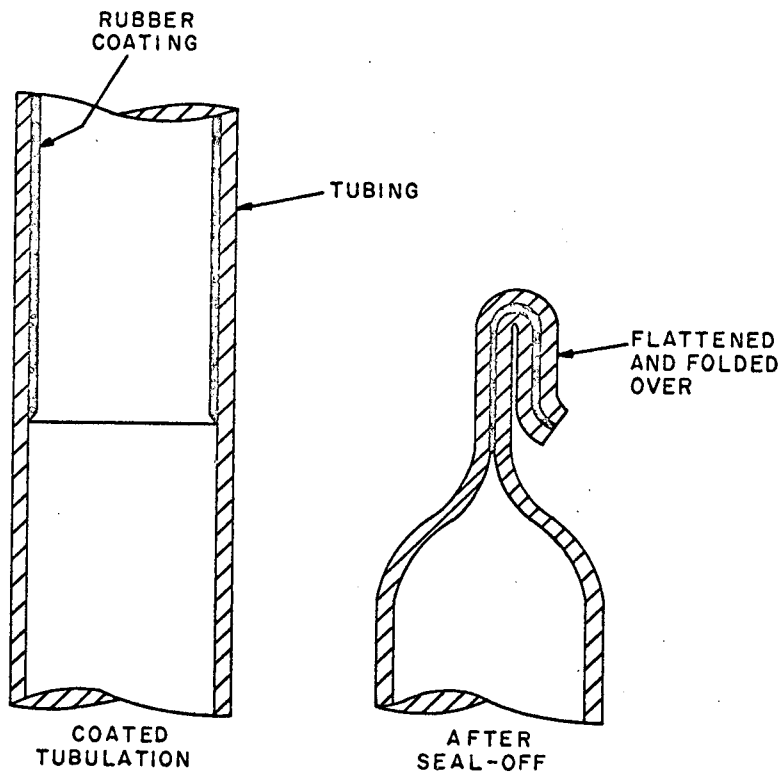
Figure 8 - Silicone Rubber Seal-Off Technique

15

TEST AND PROCESSING APPARATUS

The principal objectives for testing fuses investigated during this program were: (1) realistic evaluation of their circuit protective capabilities, and (2) comparison of the performance of various fuse designs and materials. In addition, "final design" fuses were subjected to endurance tests to evaluate fuse durability. Circuit parameters influence fuse operation in important ways: i.e., circuit parameters determine fault current rise time, the maximum fault current, and the transient overvoltage and energy the fuse must accommodate during the transition stage. Therefore, circuit parameters were kept constant for most of the fuse tests performed.

TEST STATION OPERATION

Since one principal application of such fuses would be the protection of solid-state devices, the fuse test current was passed through silicon controlled rectifiers (SCR's) which also served to switch the fault current during testing. The test station design is represented by the circuit diagram shown in Figure 9. This diagram shows the complete circuit with the exception of details for power supply switching, safety interlocks, instrumentation and lamp load switching. The logic circuits are shown in Figures 10 and 11 and their functions are described in the following section.

The "normal" circuit modes for fuse tests are represented by lamp bank R1, rectifier SCR-4 and the fuse under test, F1. When the normal current is turned on, the bypass through fuse F4 is actuated briefly to avoid fuse F1 firing due to the high "inrush" current of lamp bank R1.

When the fuse is test-fired, the simulated "fault" current is passed through fuse F2, variable resistor R2, rectifier SCR-1 and thus through fuse F1. When fuse F1 fires, the transient overvoltage appearing across F1 is used as a signal to actuate the clamp logic circuit which, after a suitable time delay actuates rectifier SCR-2. This clamp circuit diverts circuit energy from fuse F1 when the fuse arc persists. If the arc extinguishes, the current through SCR-1 and SCR-4 will commutate off after 10^{-5} to 10^{-4} second and, therefore, no current will flow through SCR-2. The primary purpose for fuse F2 is to open the high dc fault current when it is passed by the "clamp" circuit. Thus, the circuit breaker does not require the capability of opening these heavy currents, but needs only to open the normal circuit current. Fuse F2 is selected such that it will not open if SCR-1 and SCR-4 commutate; therefore, fuse F2 is of larger I^2t capacity than fuse F1.

16
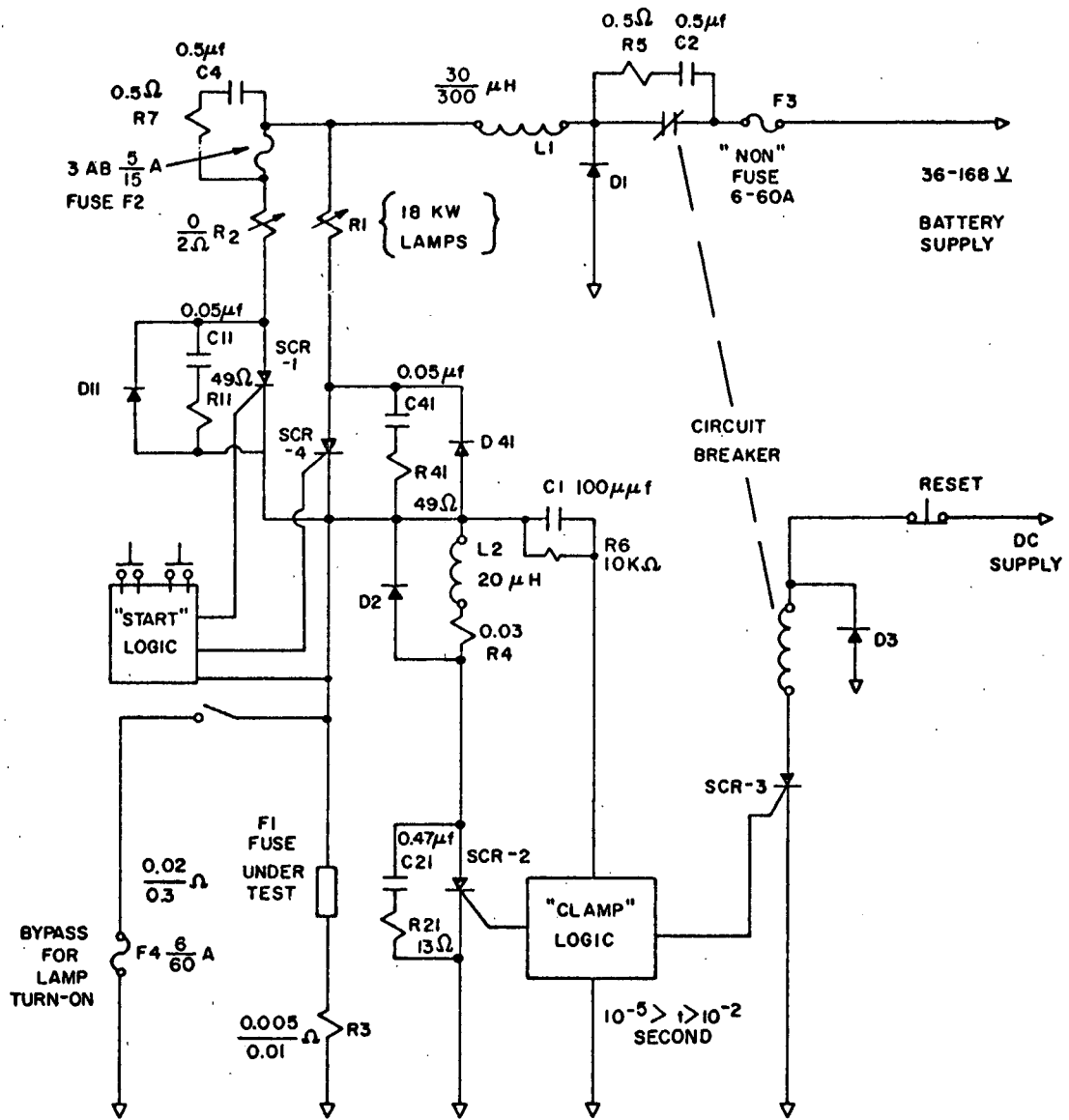
where:

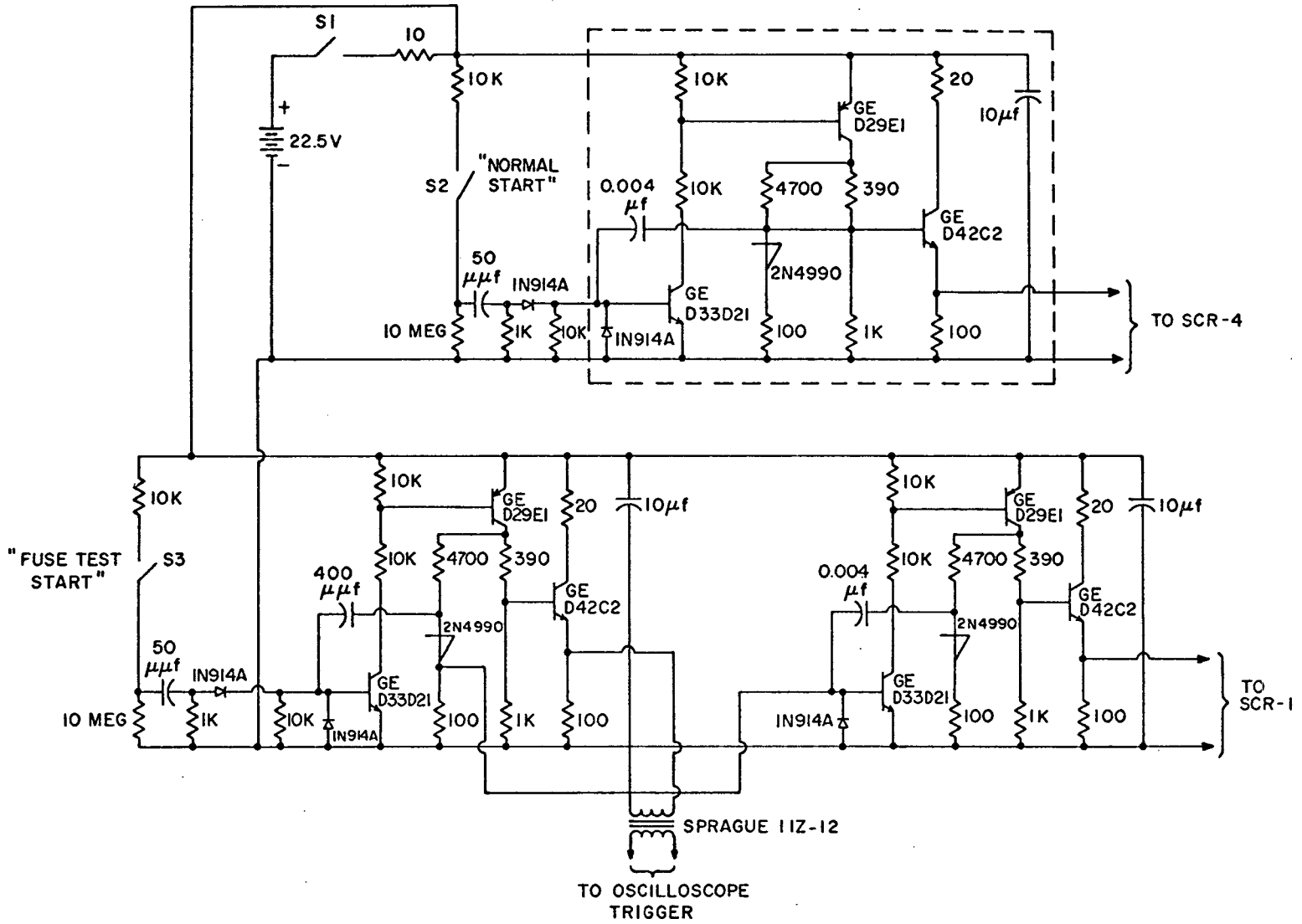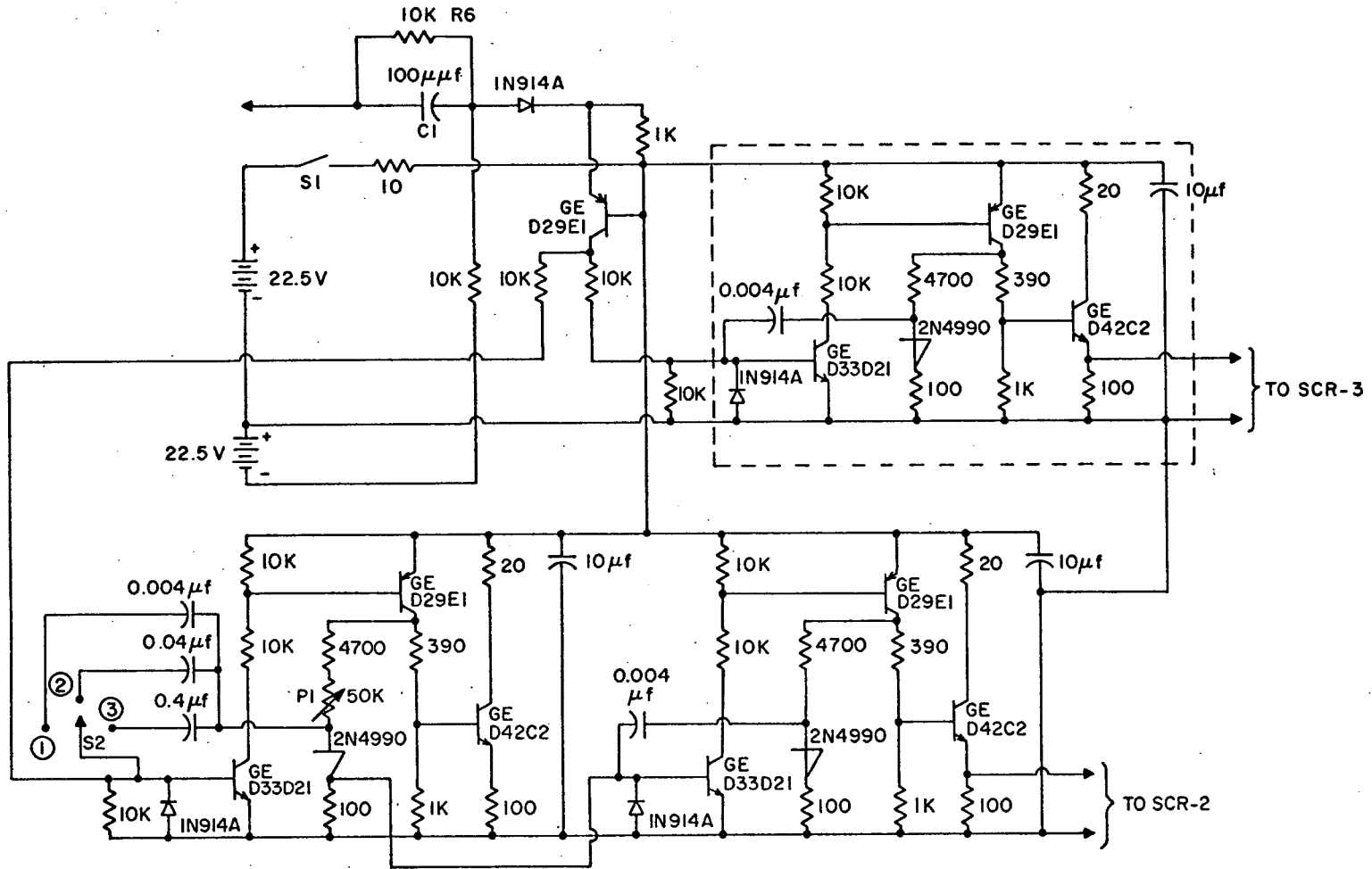|			
SCR-1, SCR-4	=	C158E	Rectifier (GE)
SCR-2	=	C158PB	Rectifier (GE)
SCR-3	=	2N3275	Rectifier (FSC)
D1	=	A96C	Rectifier (GE)
D2	=	1N4511	Rectifier (GE)
D3, D11, D41	=	1N1348	Rectifier (GE)

Figure 9 - Test Section Circuit Diagram

Figure 10 - Start Logic Circuit Diagram

NOTE:

S2 = Time delay range selector switch

Position 1 = 10^{-4} to 10^{-5} second range
Position 2 = 10^{-4} to 10^{-3} second range
Position 3 = 10^{-3} to 10^{-2} second range

P1 = Variable resistor to adjust time delay for the range selected.

Figure 11 - Clamp Logic Circuit Diagram

Circuit damping, as required, is provided for all switching elements of the circuit. Rectifiers SCR-1, SCR-2, and SCR-4 have RC "snubbers" designed to limit the current and voltage rates of rise over the contemplated range of inductance. Overvoltage is heavily damped for fuse F2 and the circuit breaker contacts. Inverse overvoltage protective diodes are provided for SCR-1, SCR-4, L1, L2, and the circuit breaker coil.

LOGIC CIRCUITS

The start logic and clamp logic circuits are shown in Figures 10 and 11, respectively.

The start logic module supplies a "start" current pulse to actuate SCR-4 and SCR-1, when S2 and S3 are actuated, respectively. The 'Fuse Test Start" circuit also supplies a trigger pulse to synchronize the oscilloscope used to monitor the fuse operation, and provides a few microseconds delay in the "start" pulse so the entire fuse test may be observed on the oscilloscope.

The circuit is designed as three basic modules, plus connecting circuitry and a battery power supply. A basic module is shown within the dashed lines of Figure 10. This module is a simple "one-shot flip-flop" circuit driving an output stage. The relatively large current required by the SCR gate is supplied from a charged capacitor (10 μf).

The clamp logic module supplies current pulses to actuate the "clamp" rectifier, SCR-2, and SCR-3, which operates the circuit breaker. The "clamp" pulse is provided with a variable time delay adjustment by switch S2 and variable resistor P1 as noted in Figure 11.

The same three modules are used for both logic circuits except the time delay adjustment described above is incorporated in one module. Small batteries supply dc power for this low-drain circuit, with one battery supplying additional voltage to provide a -45 volt bias which the input signal from the fuse must exceed in order to initiate the clamp logic. This prevents clamp logic initiation by the dc voltage due to fault currents passing through the fuse "cold" resistance and viewing resistor R3. This voltage should not exceed 30 volts.

BATTERY POWER SUPPLY

This power supply consists of fourteen 12-volt lead-acid (automotive) batteries in series, to provide up to 168 volts. By suitable switching,

12-volt steps from 0 to 168 volts are available. This supply can provide up to 1000 amperes and had a comparatively low internal inductance of approximately 15 μH.

The complete fuse test station is illustrated in Figure 12. The "Fuse Under Test" is enclosed in a box which would minimize mercury vapor leakage in case of a fuse failure. The oscilloscope is used to monitor the fuse current and voltage.

PROCESSING EQUIPMENT

Existing vacuum equipment was adapted for use in processing these fuses, i.e., for evacuating fuses and loading or unloading the mercury fill. The processing station depicted in Figure 13, consists of a mechanical vacuum pump, liquid nitrogen trap, vacuum gage, glass valve, and rotatable glass mercury-loading adapter. The glass assembly is heated by heating tape* to "outgas" the glass and to redistill mercury to obtain mercury of very high purity when desired (no improvement in fuse performance could be noted when commercial triple-distilled mercury was redistilled). The liquid nitrogen trap improves vacuum pressure as well as effectively preventing mercury from contaminating the vacuum gage and pump.

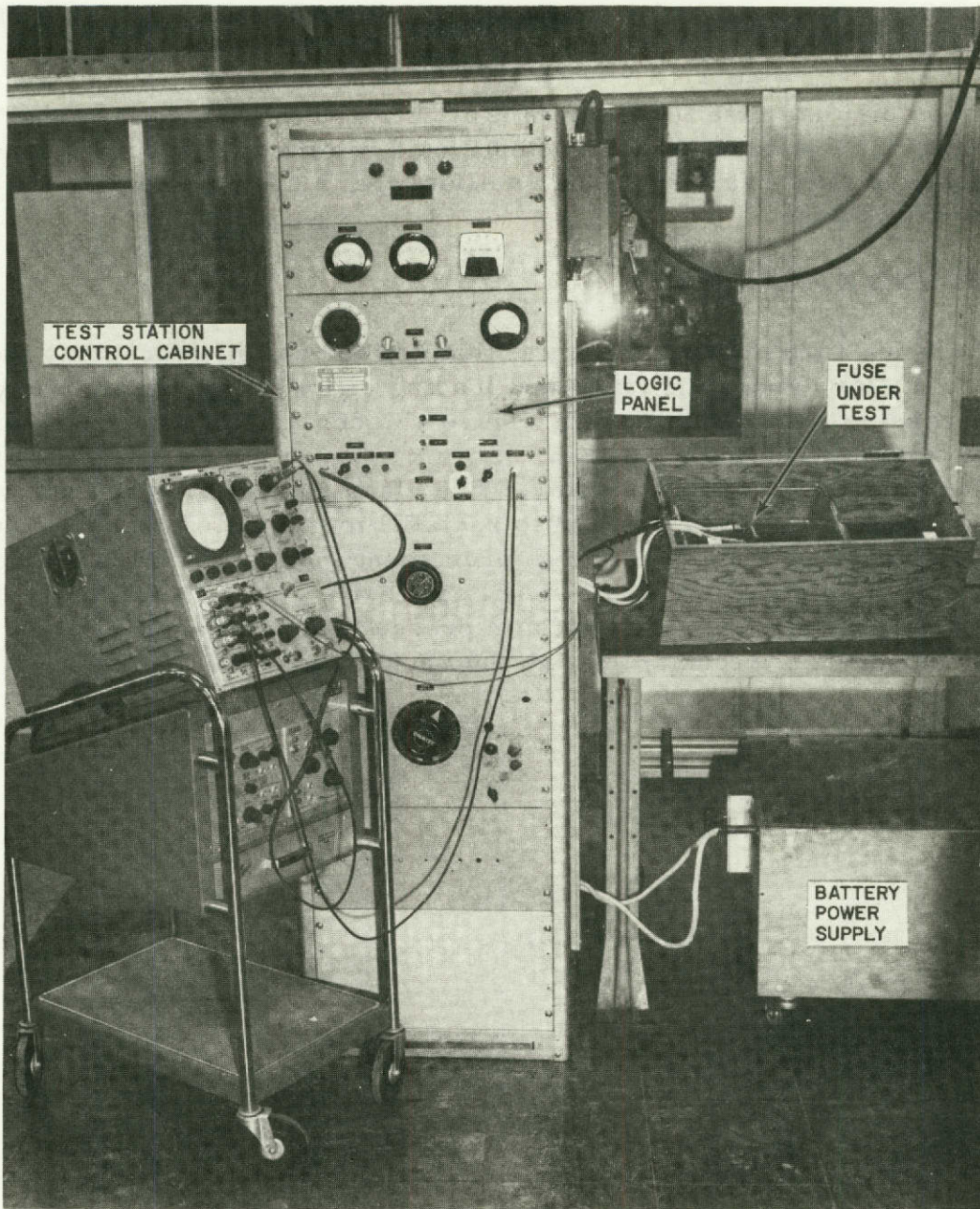*"Briskeat" No. B-2 1/2 tape, Briscoe Mfg. Company, Columbus, Ohio

TEST STATION
CONTROL CABINET

LOGIC
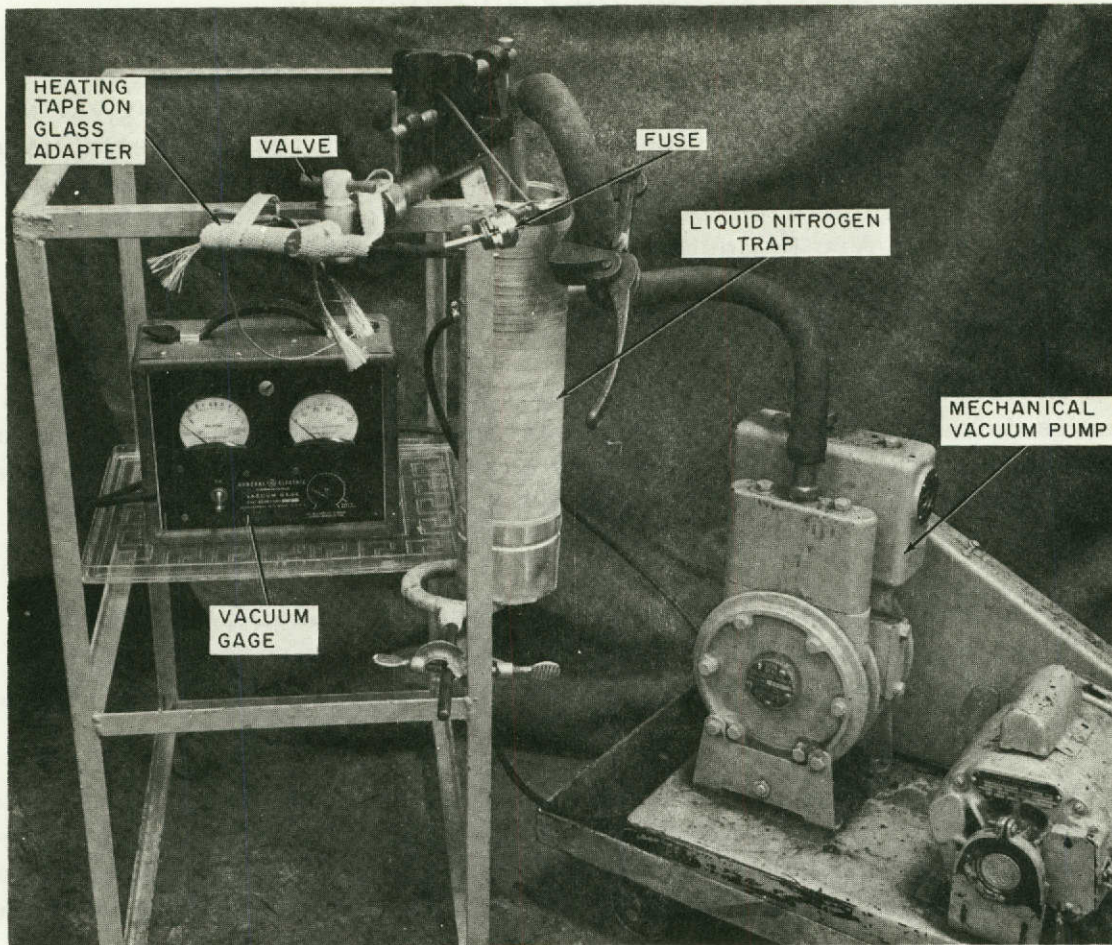PANEL

FUSE
UNDER
TEST

BATTERY
POWER
SUPPLY

Figure 12 - Complete Fuse Test Station

Figure 13 - Fuse Processing Apparatus

TEST PROCEDURES AND RESULTS

For purposes of evaluating fuse performance and comparing various fuse configurations, a standardized set of test procedures were established with NASA concurrence. These test procedures are described below and test results are summarized under three headings: "Circuit Protective Capability", "Fuse Arc Extinction" and "Fuse Channel Erosion".

FUSE EVALUATION PROCEDURE

The first step is a determination of the fuse rated current I_o. This current is defined as the steady-state current which will cause the fuse to fire within 30 to 180 seconds. A steady current of $2 I_o$ will cause the fuse to fire within one to five seconds, and $0.8 I_o$ current will not cause the fuse to fire.

The second step is a determination of the I^2t capability of the fuse, where "I" is the rms current and "t" the length of time current I passes through the fuse. This measurement was made at currents of $5 I_o$, $10 I_o$, and $20 I_o$.

The rms current and time were measured from photographed oscilloscope traces of the fuse tests. A photograph of typical oscilloscope traces is shown at the top of Figure 14, and for more clarity, the current and voltage traces are redrawn separately at the bottom. Three traces are recorded - one to measure the "fault" current, one the arc current, and one the voltage across the fuse. The upper trace in the photo records only the smaller currents of the fuse arc state -- typically 3 to 25 amperes -- and permits accurate measurement of arc current. The lower trace records current at a resolution typically 1/10 that of the upper trace.

The current is determined graphically by dividing the current waveform into sinusoidal, triangular and rectangular area segments, and using factors of $1/\sqrt{2}$, $1/\sqrt{3}$ and 1 times maximum current for the respective segments. The I^2t "let-through" is determined from total rms current passed before the fuse fires, squared and multiplied by the time in seconds from test initiation until the fuse fires.

The third step is the determination of arc extinction threshold voltage. This is defined as the highest fuse voltage at which the arc will self-extinguish within 10^{-3} second, at least 4 out of 5 test firings. The arc extinction is shown in Figure 14 where the arc persisted approximately 0.5×10^{-3} second. The arc also frequently extinguishes at the end of the "transition" stage, as depicted for a typical fuse test in Figure 15.

24
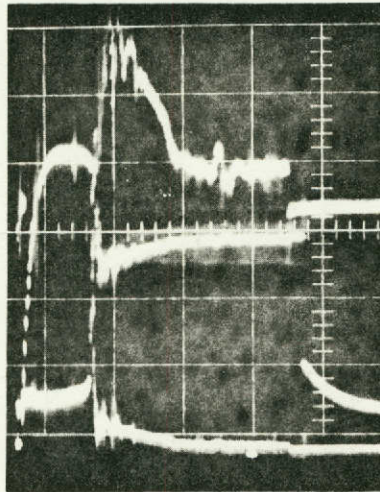
(a) Photograph of Oscilloscope Traces
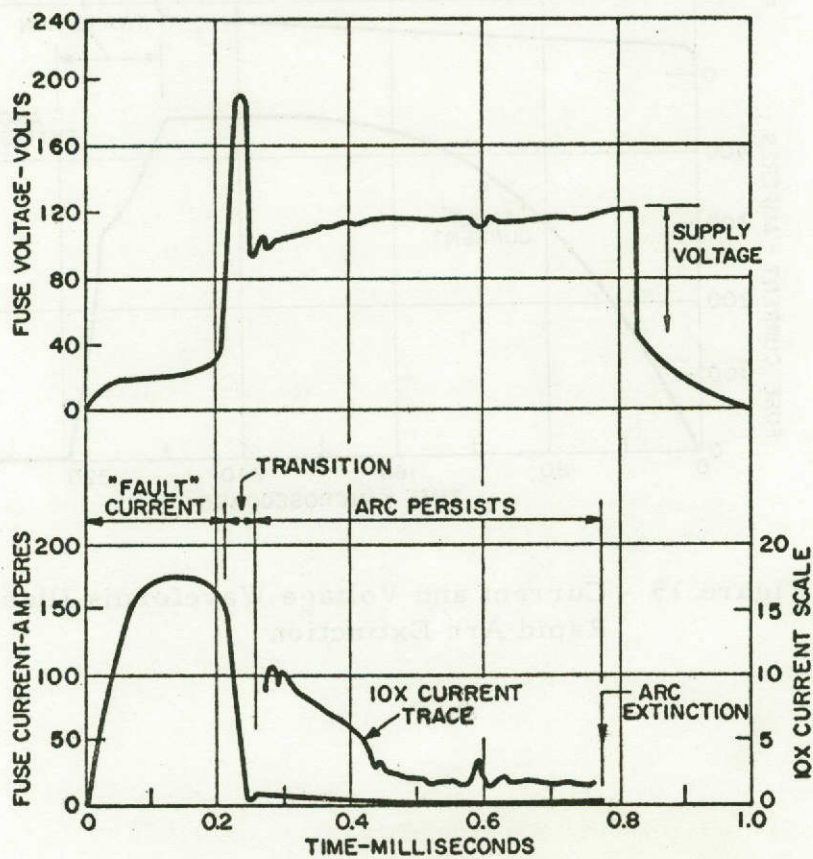
(b) Waveforms Separately Redrawn

Figure 14 - Current and Voltage Waveforms for a Typical
Fuse Test
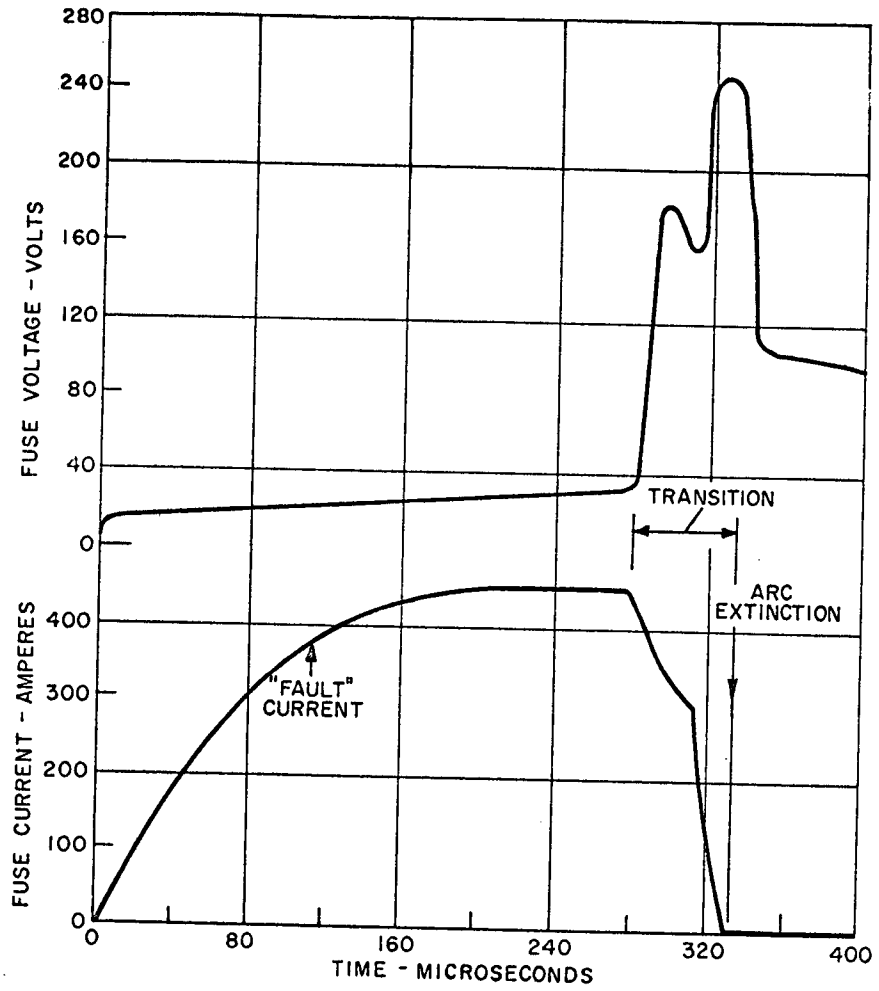
Figure 15 - Current and Voltage Waveforms Illustrating
Rapid Arc Extinction

The fuse voltage just before arc extinction is defined as the threshold voltage, and is measured from photographed oscilloscope traces. The test for arc extinction is performed for fuse currents at $2 I_o$, $5 I_o$, $10 I_o$, and $20 I_o$.

For purposes of evaluating fuse channel erosion other measurements and calculations were made. The fuse channel diameter was determined periodically during all fuse tests by measuring the electrical resistance of the mercury in the fuse channel when the fuse current is $0.8 I_o$. The average mercury temperature is approximately 150°C under these conditions, so a value of resistivity of 1.1×10^{-4} ohm-cm is used. The changes in resistance are inversely proportional to the changes in channel cross-sectional area, so resistance changes are plotted as depicting channel erosion.

The thermal energy to which the fuse channel is subjected is measured from the photographed oscillograph traces of voltage and current. During the "transition" stage, energy is dissipated at a very high rate for as long as 10^{-4} second. It is reasoned that 2/3 of the total transition energy appears as heat energy at the fuse channel walls (refer to report NASA CR-73868, p. 38). When the fuse arc persists after the transition stage, all the arc energy is absorbed by the walls, and these factors are applied to the energy dissipation calculated. Effectively, negligible energy is dissipated in the fuse channel before the fuse fires.

The rms current and voltage are determined as described earlier in this section. The energy in joules dissipated for a stage of fuse test operation, as depicted by the oscilloscope waveforms, then is (volts) x (amperes) x (time). This energy then can be calculated from any photographed oscilloscope trace, or energy can be estimated reasonably well from fuse test data, if the arc extinction rate is observed. The latter is feasible because the energy of the transition and arc stages are reasonably consistent for a given fuse in a given circuit if circuit voltage is constant.

CIRCUIT PROTECTIVE CAPABILITY

The primary protective function of current limiting devices such as those investigated here is to limit the energy that other circuit devices are subjected to during circuit faults. The energy limit for solid-state or other circuit devices due to joule heating is usually expressed as an I^2t rating, which, when multiplied by device impedance, gives the actual joule heating. This applies for a fault current time range from approximately 10^{-2} to 10^{-5} second. For shorter times, time rates of change for current or voltage becomes important, and for longer times, heat capacity and heat conduction of the structural members become important.

The average time responses (calculated and measured) of several fuse cylindrical channels used for this program are shown in Figure 16. The calculated values assume that all I^2R heat is absorbed by the heat capacity of the mercury, which appears to hold true at times of 2×10^{-3} second or less. For longer periods heat conduction to the channel walls becomes a factor, as illustrated in Figure 16.

The appreciable deviation from calculated values for the 0.75- and 0.070-mm channels is due, in part, to the comparatively high pressure applied to the mercury by the heavy springs of the end buffer structure of the fuse (refer to "External Fuse Structure" sub-section). Less mechanical pressure is applied by the fuse structure for smaller channel devices, therefore, the mercury boiling temperature is lower. The calculated values assume a pressure of 1.5 atmospheres.

A summary of test data on I^2t performance, rated current and arc extinction voltage are reported in Table I. The I^2t data, including the range, are only for tests of less than 2×10^{-3} second duration.

FUSE ARC EXTINCTION AND IMPEDANCE

The earlier fuse work had indicated that small fuse channels would provide much higher arc extinction voltage than larger channels. This has been borne out, both in the fuse operating data shown in Table I and in further analytical work (refer to Appendix A). The trend of the recent fuse operating data for alumina is summarized as "Present Data" in Figure 17, along with curves showing the latest analytical treatment labeled "Present Theory". Prior experimental data from the NAS12-675 program is labeled "Alumina" and "Sapphire", and prior analytical work is represented by the bars labeled "H".

The trend of the "Present Data" arc extinction voltage, as defined for the "Fuse Tests Procedure" sub-section, is the voltage at which 80 percent of the fuse tests indicate arc extinction. Assuming that the "Present Theory" curve represents the higher voltage at which 50 percent of the arcs would extinguish, the agreement between theory and experience looks very good. Based on observations made during fuse tests, the attaining of a probability of arc extinction higher than 80 percent would require correspondingly reduced fuse voltage. On the other hand, allowing arc times longer than 10^{-3} second will tend to increase the allowable fuse voltage for a given arc extinction probability.

TABLE I - SUMMARY OF DATA OBTAINED FOR FUSE CHANNELS OF VARIOUS SIZES

Fuse Channel Dia. x Length (mm)	No. Channels	Rated Current (A)	I^2t Average (A^2s)	Range	Arc Extinction (V/cm)	Fuse Cold Resistance (ohms)
0.18 x 8	8	15	40	25-50	130*	0.052
0.20 x 9	6	15	40	30-60	120	0.045
0.28 x 8	4	15	60	50-70	80	0.030
0.35 x 4	1	8	5	3-8	-	0.046
0.45 x 7.5	1	10	25	15-45	65	0.045
0.050 x 10	1	15	35	25-50	50	0.050
0.70 x 25	1	18	120	90-150	30*	0.060
0.75 x 23	1	20	160	90-200	44	0.050
1.2 x 25	1	35	500	400-600	36	0.023
0.2 x 10	2	5	2	1-3	120	0.140
0.75 x 23	2	40	580	500-700	45	0.026

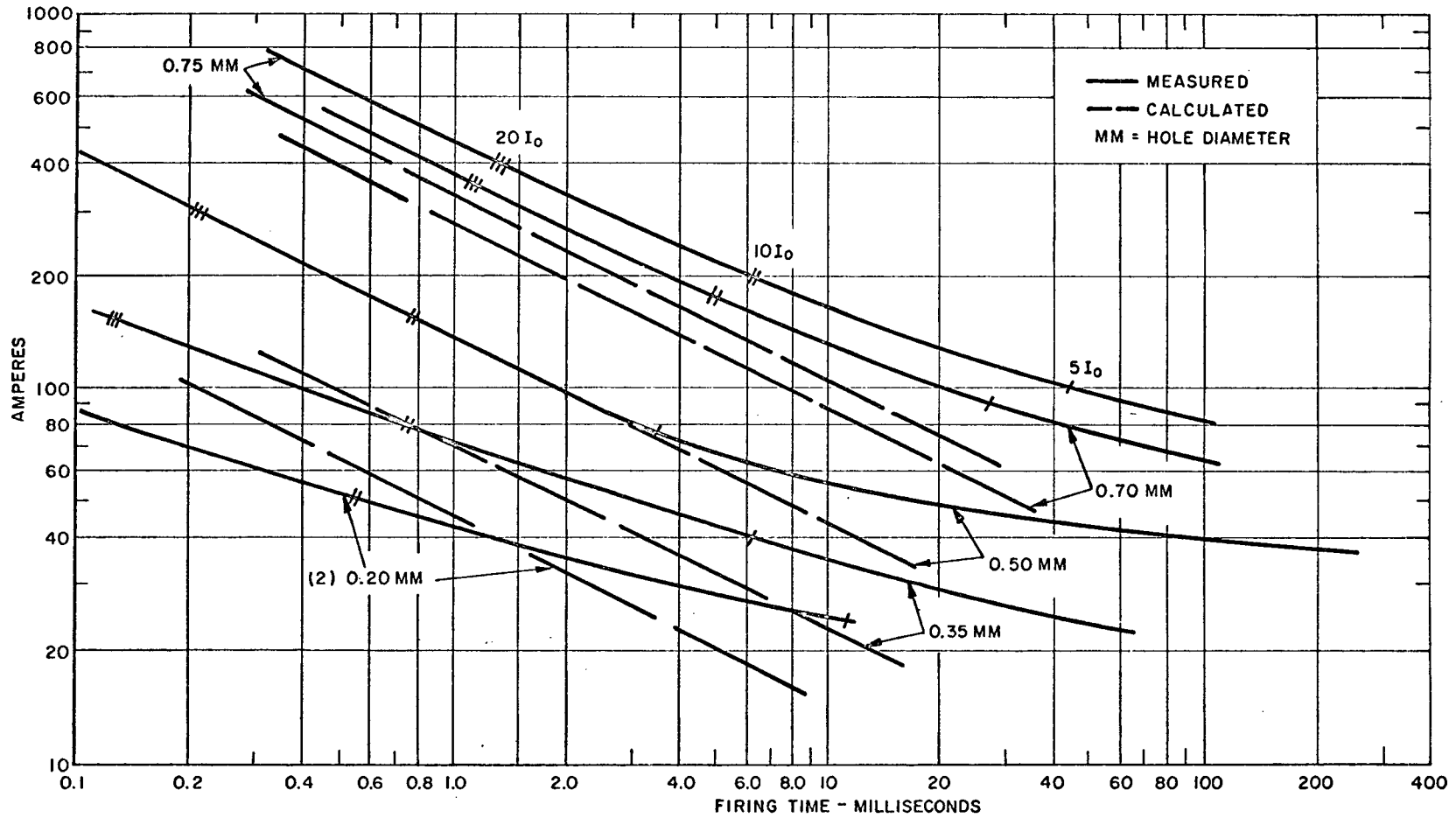*Beryllia channel material. Other channels are alumina
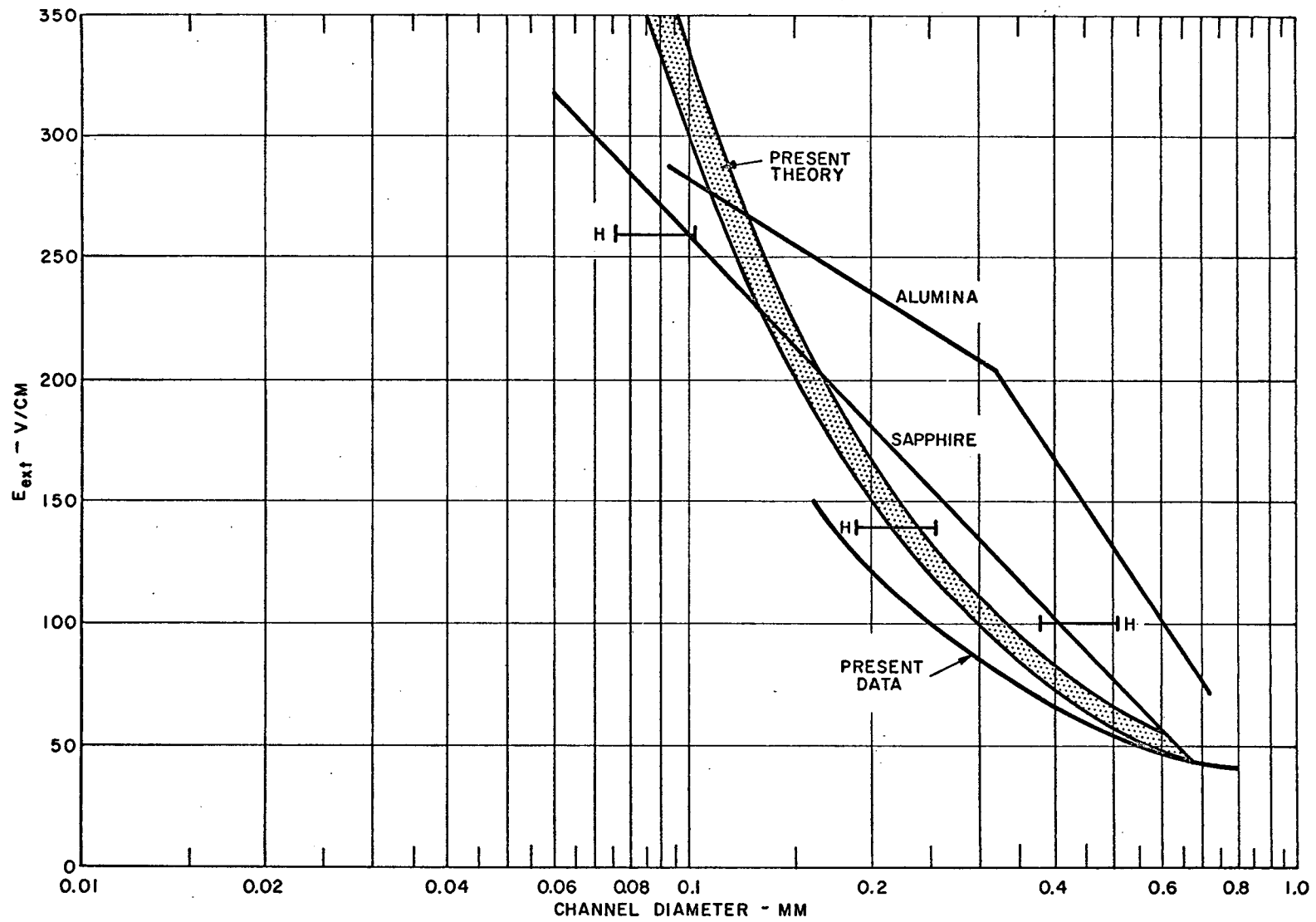
Figure 16 - Time Response for Various Fuse Channels

Figure 17 - Analytical and Experimental Fuse Performance vs. Channel Size

The data obtained concerning the impedance of the "stable" arc are somewhat elusive, due to the arc instability in the first millisecond of arcing. Most fuse tests were limited to 1 ms or less, but those which were allowed to arc for longer periods indicate somewhat more stable arc behavior with time. Thus the data considered representative of stable arc behavior are those exhibited after 0.3 ms or more of arcing.

The impedance ratio between the observed arc impedance and "cold" (liquid mercury) resistance conforms reasonably well to the analytical study of the arc reported in Contract Report NASA-CR-72868 (p. 41). The 0.75-mm channel fuses range from 150 to 300 in impedance ratio with approximately 220 as the most typical ratio. The 0.2-mm channel fuses range from 350 to 700 impedance ratio with 500 as the most typical ratio.

FUSE CHANNEL EROSION

The two factors involved in enlarging or eroding the fuse channel are, thermal energy which melts or vaporizes material from the channel walls, and mechanical shock which causes the insulating material to crack or chip. Thermal erosion is a more important factor for devices that are to withstand 1000 operations (the desired objective). Therefore, these devices were intentionally over-designed, mechanically, to minimize damage caused by mechanical shock. However, fuses fabricated by glass molding techniques usually experienced some mechanical damage to the fuse channel. The all-ceramic fuse design shown in Figure 4 did not indicate mechanical erosion of the channel.

The erosion behavior of a representative group of glass-molded fuses is depicted in Figure 18. As noted in the figure, two of these fuses (MT-1 and MB-5) experienced visible mechanical damage. Fuses S-20 and A-22 experienced a minimum of erosion, if any. The resistance change probably represents cleaning "debris" from the channel. Fuse MB-7 had 250 fuse tests performed, and the data indicated that major erosion was thermal, although some mechanical damage was visible in X-rays taken when the device was filled with mercury. Under similar test conditions, fuse A-7 showed more rapid thermal erosion in comparison to fuse MB-7. This probably illustrates the better durability of beryllia as compared to conventional alumina (99 percent pure).

The data on fuse channel erosion for the ultra-pure (99.9 percent) alumina indicate performance comparable to beryllia. Test results for the four fuses tested extensively are listed in Table II.
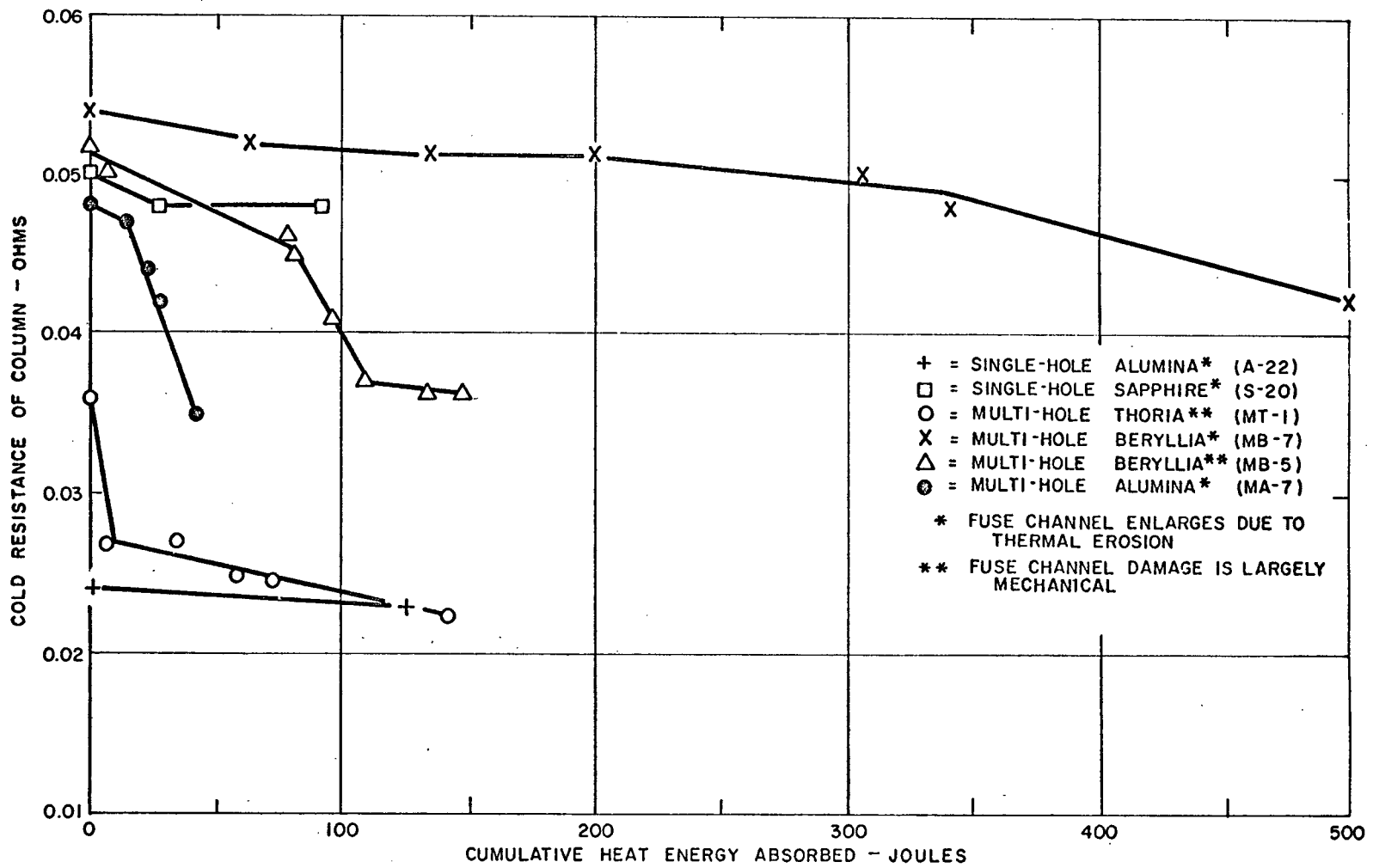
Figure 18 - Test Results for Self-Healing Fuses

TABLE II - ENDURANCE TEST DATA FOR ALUMINA AND BERYLLIA FUSES

Fuse No.	Channel Dia. (mm)	Length	Material	Wall Area $cm^2 \times 10^{-2}$	Typical Energy Density[**] (kW/cm^2)	No. Tests	Erosion Start (ohms)	End	Change (Percent)
MB-7[*]	0.18	8.0	BeO	136.2	5.8	250	0.052	0.042	20
B-1	0.70	20.0	BeO	44.1	4.8	500	0.058	0.056	4
L-16	0.45	7.5	Al_2O_3	10.6	6.6	500	0.045	0.045	0
L-28	0.75	23.0	Al_2O_3	54.2	4.1	400	0.052	0.048	8

[*]MB-7 had 8 channels. Other fuses were single-channel devices.

[**] For fuse tests where the arc persists for 10^{-3} seconds.

Since the accuracy of the energy measurements may be no better than ± 20 percent, the apparent discrepancy between energy density and erosion rate for L-16 and L-28 may be largely measurement error. The trend of the data indicates that an energy density of 5 kW/cm^2 is the approximate limit for beryllia or high purity alumina. The test duration for all these tests (before the fuse voltage was "clamped") was approximately one millisecond. Most tests for fuses MB-7 and L-28 were conducted at 120-150 circuit volts, and fuses B-1 and L-16, which exhibited much lower arc extinction threshold voltages, were tested at 50 volts.

The following data listed in Table III were obtained prior to shipment of 24 fuses to NASA for evaluation.

TABLE III - FINAL TEST DATA FOR FUSES SHIPPED TO NASA FOR EVALUATION

Fuse No.	Fuse Channel Dia. x Length mm	Material **	Fuse Rating Amps.	Volts	Notes
A-22	1.2 x 25	Al_2O_3	35	75	1
A-23*	0.5 x 20	Al_2O_3	20	100	1
B-1	0.7 x 20	BeO	18	50	1
B-2	0.7 x 25	BeO	18	75	1
L-22	0.75 x 20	U	20	75	1
L-26	0.75 x 20	U	20	60	1
L-27	0.75 x 20	U	20	75	1
L-28	0.75 x 23	U	20	90	2
L-29*		U	40	80	2
L-30		U	20	90	2
L-31*		U	40	100	2
L-32		U	20	100	2
L-33		U	20	100	2
L-34		U	20	90	2
L-35*		U	40	90	2
L-36		U	20	100	2
L-37		U	20	90	2
L-38	0.75 x 23	U	20	90	2
MA-6	0.28 x 8	Al_2O_3	5	70	3
MA-8*	0.15 x 10	U	5	80	3
MA-9*	0.15 x 10	U	5	50	3
MB-6*	0.18 x 8	BeO	5	75	3
MB-7*	0.18 x 8	BeO	5	90	3
S-20	0.5 x 10	Sapphire	15	50	1

NOTES:

* - Denotes fuses with two channels. All other fuses have one channel.

** - U denotes ultra-pure alumina.

1 - External fuse structure sealed with expoxy cement, considered the least reliable structure.

2 - All-welded structure, considered highly reliable.

3 - "0"-ring sealed structure, considered moderately reliable.

DISCUSSION OF RESULTS

In discussing the results in this section, four major areas are treated in the order indicated:

(1) Factors in circuit protection.
(2) Arc extinction characteristics and arc impedance.
(3) Erosion of the fuse channel.
(4) Design parameters for self-healing fuses.

FACTORS IN CIRCUIT PROTECTION

These devices inherently provide circuit protection superior to conventional fuses in two respects: 1) the arc impedance is usually large enough to limit current during the "arc state" to approximately normal circuit current, 2) the fast-switching capability can very quickly clear short-term minor faults (such as occasional commutation failures in SCR-operated inverter circuits) without other circuit protective devices operating, and thus, will exhibit only very momentary circuit interruption. With respect to arc impedance, conventional fuses exhibit comparatively low impedance and long persistence time (the order of 10^{-2} second), although special "rectifier" fuses tend to exhibit much shorter arc persistence -- less than 10^{-3} second. The high impedance of the self-healing fuse arc also allows the use of a protective switch of relatively low current interrupting capability; and, for mechanical switches, this becomes a light fast-acting switch compared to the heavy contactors required to open large fault currents where no fuse is used.

The I^2t capability of these devices can be adjusted over a large range, depending upon whether a multi-hole or single-hole design is used, or what "cold" resistance is feasible for the fuse. For example, eight-channel fuses with 0.18 x 8 mm channels have the same resistance and arc extinction capability as single-channel fuses with a 0.75 x 23 mm channel, but I^2t is four times higher for the latter. The I^2t can be calculated with reasonable accuracy as $I^2t \simeq 5 \times 10^6 \ A^2$ Amp^2 seconds, where A is the hole cross-sectional area in cm^2. This is the basis for the "calculated" lines shown in Figure 15, where the dashed lines are current and time for constant I^2t.

As can be seen from the data in Table I, there is generally a 2:1 range in I^2t performance for devices of essentially the same hole diameter. Much of this difference can be explained by the small variations in diameter, since I^2t would vary as the fourth power of the hole diameter. The larger diameter devices also tend to have larger I^2t than the calculations indicate. This is

probably due to the much larger wall area of the channel, which is both larger and longer for the same current and voltage rating.

Data on I^2t performance was obtained using two circuit conditions. Most test firings were performed with the fuse at an equilibrium temperature with normal circuit current flowing through the fuse and with the fuse electrical connections (standard fuse "clips") at approximately $80^\circ C$. Several fuses were also test fired "cold" with no circuit current flowing prior to the "fault" current. As would be expected, the I^2t rating was about 25 percent higher for the fuses fired "cold" as compared to "normal" conditions. The data shown in Tables I and II represent "normal" current conditions.

ARC EXTINCTION CHARACTERISTICS AND ARC IMPEDANCE

This work has established a better understanding of the confined metal-vapor arc, both as phenomena and in terms of device design parameters. Due to the erratic nature of the arc, design parameters are not precisely defined, but can be approximated reasonably well.

Data most representative of arc extinction behavior are shown in Figure 17 and Table I. There are some additional variations of arc extinction behavior. A substantially lower arc extinction threshold voltage is exhibited by larger single-channel beryllia fuses as compared to the alumina devices. This is shown in Table I for the 0.70-mm diameter channel. The eight-channel, 0.18-mm diameter beryllia fuses were quite comparable to alumina fuses, however. The single-channel beryllia data then may be a statistical variation in the data (there were two fuses tested, Nos. B-1 and B-2).

The introduction of impurities from the fuse channel into the mercury would probably produce more reduction in arc voltage for alumina than beryllia, since aluminum has a first ionization potential of 6.0 versus 9.3 for beryllium and 10.4 for mercury. Thus the lower arc voltage for the two single-channel beryllia devices is not readily explained except as a statistical variation. The introduction of impurities could explain the reduction of arc extinction voltage with time as fuses are life tested, however. This reduction occurred for three of the four fuses tested for over 250 firings (refer to Table II). Fuse L-16, which did not experience the reduction in arc extinction voltage, was tested at 48 circuit volts for most tests, and experienced no measureable fuse channel erosion. The other three fuses experienced arc extinction voltage reduction of approximately 10 to 15 percent.

38

FUSE CHANNEL EROSION

The data obtained during this program indicate that, in terms of fuse channel erosion, at least 500 fuse operations are feasible for self-healing fuses designed for this work. The energy density which ultra-pure alumina or 99 percent pure beryllia will tolerate for 1 ms is approximately 5 kW/cm^2 (refer to Table II). The earlier fuse work indicated that sapphire (virtually 100 percent pure crystalline alumina) is at least as durable as ultra-pure alumina. Thus these three insulators are regarded as esentially equal in durability, as fuse channel materials.

The data obtained do not indicate limits of energy tolerance for longer times, but the acceptable energy would logically be proportionally lower for longer arc persistence times. Since relays or other mechanical devices usually require two or more milliseconds to operate, the use of these fuses with mechanical switches would require a more conservative fuse design or a suitable voltage derating of the fuse (energy is usually a V^2 function).

The discrepancy in energy density versus erosion for fuses L-16 and L-28 may reflect a non-uniform distribution of energy for the longer, higher voltage fuse. If this holds true, some additional derating of fuses may be required for operation at higher voltages.

Arc extinction is also a factor in fuse channel erosion, because about half of the energy impinges on the fuse channel during the one millisecond arc stage for the data cited in Table II. Thus, the energy is essentially half as great for the arc extinction case as for the arc persistence case; therefore, voltage derating, which increases the likelihood of arc extinction, is doubly effective in reducing the rate of fuse channel erosion.

The fault current I is also a strong factor in channel erosion because the energy due to a fault would logically fall between I and I^2 as a function. The reason being that energy of the "transition" stage is a product of rms voltage and current (refer to "Fuse Evaluation Procedure" subsection) and the voltage is the sum of circuit voltage plus L di/dt overvoltage resulting from the rapid decrease in current during the transition stage. The overvoltage may be 1 to 3 times circuit voltage for a fault current of 20 I$_o$, while overvoltage is usually negligible for a fault current of 2 I$_o$ in a low-inductance circuit. This is because higher current allows more energy to eject mercury from the channel, producing a shorter transition and a much higher di/dt for higher current faults. The larger single-channel fuses also experience lower di/dt compared to smaller multi-channel fuses because the mechanical forces act more slowly on the larger mass of mercury.

The circuit inductance also has some effect on the level of "transition" stage energy for a given fuse firing because of inductive overvoltage being proportional to circuit inductance. Added inductance was provided in the fuse test station circuit (refer to Figure 9) to allow evaluation of this factor on fuse arc extinction and fuse channel erosion. However, the limited data obtained at higher inductance did not provide any conclusive indications of the effect of higher inductance in the faulted circuit.

FUSE DESIGN PARAMETERS

The best established fuse design parameter is the cold resistance for the mercury in the fuse channel, which is simply calculated from the resistivity of mercury at $150^{\circ}C$ (1.1×10^{-4} ohm-cm). The cold resistance for the 15- to 20-ampere fuses has been approximately 0.05 ohm for the devices tested in this program, which is about twice the resistance (or circuit power loss) of conventional "rectifier" fuses. It is advantageous fo design for higher cold resistance, since this allows the use of longer channels which leads to more reliable arc extinction and the use of larger wall areas which leads to lower fuse channel erosion.

The current rating of these fuses generally is related to the power dissipation (P) and wall area (A_w) of the fuse channel. This was found empirically to be a function approximated by the expression: $P (watts) = 100 A_w (cm^2)$. The watts are I^2R heating, where R is the fuse channel "cold" resistance and I is approximately 1.5 times I_0, the fuse current rating; i.e., the fuse will fire after 10 to 60 seconds at a steady current of $1.5 I_0$. The 100 factor is the product of the heat transfer coefficient "h" and "ΔT", the temperature drop between the mercury and the fuse channel. "h" would be the order of $0.5 \ watt/cm^2/^{\circ}C$ and "ΔT" approximately $200^{\circ}C$ to fit these conditions.

The current rating and the response of the fuse would be appreciably affected by the thermal impedance of the mechanical support structure of the fuse or electrical connections to the fuse. Such factors must be considered for any eventual application of these fuses.

The arc extinction voltage parameter for various channel diameters is depicted in Figure 17, as a function of voltage gradient in the fuse channel. There is a statistical variation of about ± 20 percent among different devices for data shown for arc extinction, as well as variations with the length of time the arc is permitted to continue. These variations in voltage become more important as the desired reliability is increased, or of less importance for lower reliability.

The exception to the arc extinction function as presented above was the performance of two 0.70-mm diameter single-channel beryllia fuses, that provided somewhat lower arc extinction voltage than other fuses tested. The other beryllia fuses, having 2 to 8 channels of 0.16 to 0.20-mm diameter, were comparable to alumina fuses with 0.20-mm channels. Both sizes of beryllia were extruded two-hole tubing obtained from the same vendor[*] with the same material specifications (99% +pure). Since the larger diameter beryllia channels also exhibited somewhat lower arc impedance, it would appear that the behavior of these devices may represent the presence of a lower ionization potential impurity in the beryllia; however, this conjecture could not be verified within the confines of this program.

[*]Brush-Wellman, Inc., Elmore, Ohio 45416.

CONCLUSIONS

Extensive self-healing fuse tests were performed in a specially designed solid-state test circuit. These tests demonstrate the superiority of these fuses in protecting solid-state devices, since they provide better energy-limiting action and faster current interruption than commercially available conventional fuses. Test data shows consistent performance, in terms of energy-limiting action, for both single-and multi-channel configurations in alumina and beryllia. The available data cover the range of 5 to 40 amperes; however, fuse performance can reasonably be projected to provide protection over wider current and voltage ranges.

It has been found that explosive mechanical forces generated by fuse operation can be contained by a fuse design embodying all-ceramic insulators pre-stressed by force-fitted external metal rings. Fuses utilizing simpler ceramic configurations molded in glass were less durable. Fuses of both designs have been furnished to NASA for further evaluation.

Life tests were conducted to demonstrate a capability of at least 500 operations where the energy impinging on the fuse channel was 5 kW/cm^2 for one millisecond.

The switching capability of these devices has been extensively evaluated and compared to an analytical treatment of mercury-vapor arcs, with good agreement. A high arc impedance, which sharply limits the current and energy of faulted circuits, has also been demonstrated. Smaller fuse channels provide both better switching performance and higher arc impedance.

A simple bellows, heavily spring-loaded and mechanically restrained to resist impact forces, adequately provides the elastic characteristics required of the fuse container. A novel technique utilizing silicone rubber was applied to seal off these devices.

APPENDIX A

SELF-HEALING FUSE THEORY

R. E. Kinsinger

In the earlier theoretical work on mercury filled self-healing fuses (see Appendix A of Contract Report NASA CR-72868), L. P. Harris has constructed steady state arc characteristics (field versus current density for fixed diameter) using a crude model. The arc energy equation, balancing Joule heating against several different dissipation mechanisms treated separately has been taken into consideration.

The cooling mechanisms considered were:

    (1) atomic conduction

    (2) electron conduction dominated by electron-neutral collisions

    (3) electron conduction dominated by electron-ion collisions

    (4) ion diffusion

    (5) radiation.

The conductivity in the channel was determined by electron-neutral collisions for: (1), (2) and (4) and by electron-atom collisions for (3) and (5). For each case, a simple temperature profile was adopted and a "characteristic" subject to the above assumptions was generated. The final characteristic for a given channel diameter was arrived at by assuming that the results of (2) - (5), with qualitatively similar temperature profiles, could be summed in a straightforward manner. The result of this summation was plotted for the high temperature - high current density regime while the result for (1) was adopted for the low temperature - low current density regime. Since the former gives a generally positive incremental resistance and the latter a generally negative incremental resistance, there is a field of voltage minimum which is a function of the channel diameter.

The value of characteristic curves is twofold. They can give a qualitative indication of the performance or failure mode of test fuses as well as providing design information through the determination of a minimum or

extinction electric field, E_{ext}, as a function of channel diameter. It was therefore, decided to improve the theoretical determination of the arc characteristics.

For the small channels ($D \lesssim 0.05$ cm) under consideration for the design and testing of this study, Harris's results provide justification for the neglect of radiation as an energy transfer mechanism. For narrow channels the arc is optically thin, and for the temperature range under consideration ($T \lesssim 1.2$ eV) the total power radiated in the continuum is small in comparison with that transported by conduction. It may be assumed that in this regime line radiation may be neglected as well.

With radiation neglected, the steady arc energy balance equation for cylindrical arcs can be written

$$\sigma(p, T)E^2 + \frac{1}{r} \frac{\partial}{\partial r} \, rK(p, T) \, \frac{\partial T}{\partial r} = 0 \qquad (1)$$

where T is a local (radius dependent) temperature, E is the arc electric field, and $\sigma(p, T)$ and $K(p, T)$ are the coefficients of electric and thermal conductivity with local thermal equilibrium assumed throughout. The first term, σE^2, provides Joule heating while the second term must include the energy transfer mechanisms (1) - (4).

The program ARC3 (a program listing is included in this appendix) is set up to solve this differential arc cooling equation in the following way. Since for a given solution E is independent of r and T, we define a new independent variable.

$$r_e = rE \qquad (2)$$

and write

$$\sigma(T) + \frac{1}{r_e} \frac{\partial}{\partial r_e} \left[r_e K(T) \frac{\partial}{\partial r_e} \right] = 0. \qquad (3)$$

The boundary conditions are given as

$$T(r = 0) = T_o$$

$$T(r = R) = T_w \qquad (R \sim \text{radius of channel}) \quad (4)$$

44

With these boundary conditions the program integrates the differential equation from the center, $r_e = 0$, to the wall and determines:

$R \cdot E \sim$ radius of arc channel $\cdot$ electric field

$$F_w/E = K(T_w) \left.\frac{\partial T}{\partial r_e}\right|_{r_e} = R \cdot E \qquad (5)$$

(energy flux at channel wall/electric field)

$$J/E = \bar{\sigma} = \frac{2}{R \cdot E} (F_w/E) \qquad (6)$$

(average conductivity of channel and temperature profiles, $T(r_e)$.)

The wall temperature may be chosen as desired. Values as widely spaced as the boiling point of mercury (629 K) and (0.2 eV = 2321 K) produce minor changes in the results.

The center temperature is parametrically varied over a run to produce results for the interesting range of current density and channel size.

Pressure is assumed uniform in the arc and is input at the beginning of the run. Pressures of one atmosphere were generally used; however, pressures as high as 10 atm made minor changes in the results.

Transport coefficients, $\sigma(p, T)$ and $K(p, T)$ are calculated in the subroutine TRANSP. Both electron-neutral and electron-ion collisions are considered in determining the conductivity, $\sigma(p, T)$. The coefficient of heat conduction, $K(p, T)$ includes electron conduction, atomic conduction, and ionic diffusion components.

Plots of $\sigma(T)$ and $K(T)$ for p = 1 atm are included as Figures 19 and 20. For Hg, the cross sections for electron-atom and ion-atom momentum transfer are somewhat in doubt; therefore, several alternatives are plotted.

Hg (1) $Q_{ea} = 3. \times 10^{-15} \, cm^2$ $\quad Q_{ia} = 1. \times 10^{-14} \, cm^2$

(2) $Q_{ea} = 6. \times 10^{-15} \, cm^2$ $\quad Q_{ia} = 1. \times 10^{-14} \, cm^2$

(3) $Q_{ea} = 3. \times 10^{-15} \, cm^2$ $\quad Q_{ia} = \infty$ (no ionic diffusion)

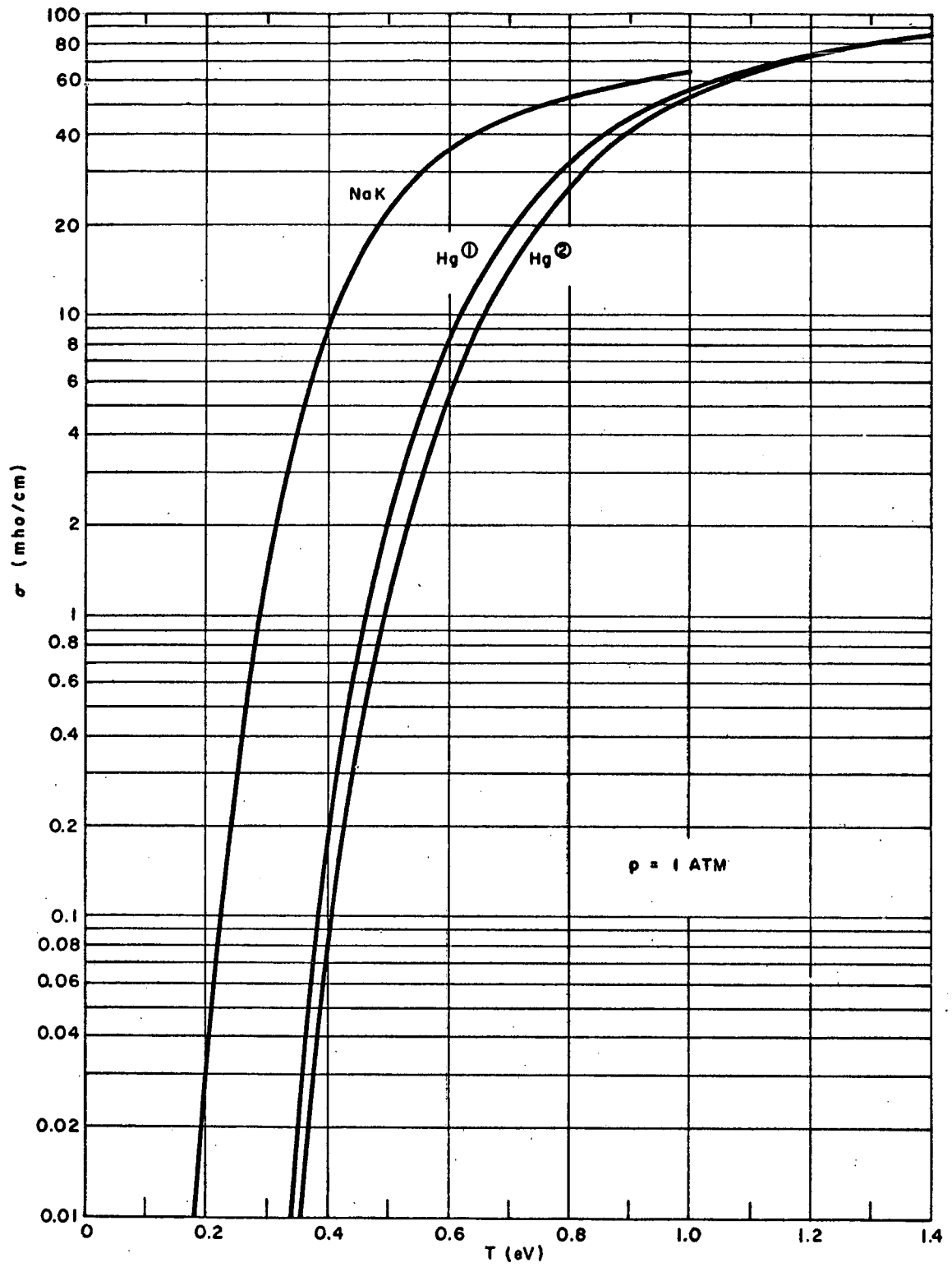Plots are also included for eutectic NaK, two atoms of K per atom of Na.

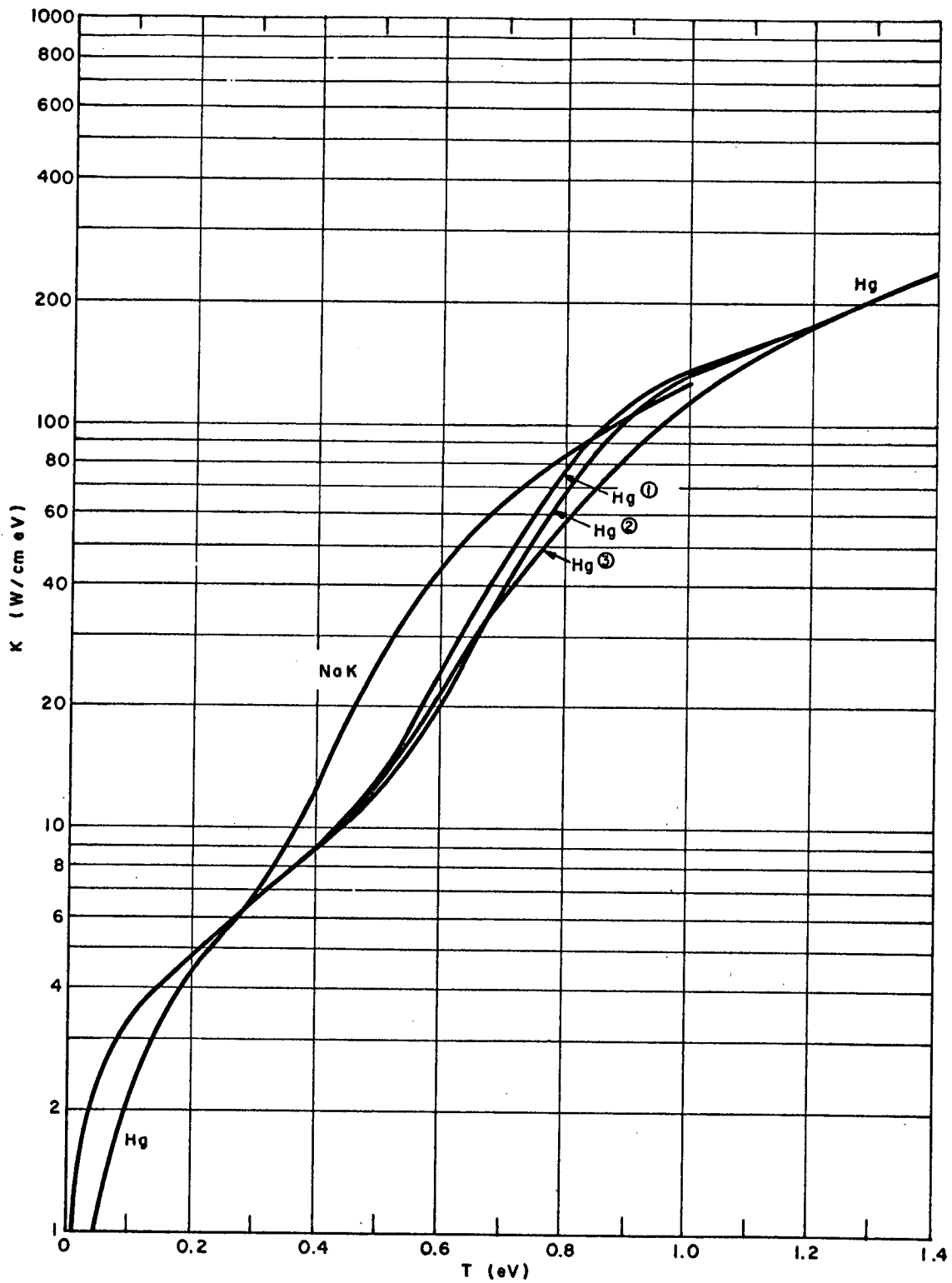Figure 19 - Calculated Electrical Conductivity for Mercury and NaK Metal Vapor Arcs

Figure 20 - Calculated Heat Conduction for Mercury and
NaK Metal Vapor Arcs

The results of ARC3 are most usefully plotted as $R \cdot E$ vs $\bar{\sigma} = J/E$. Plots of this type are given for Hg (1) with $T_W = 629$ K and eutectic NaK with $T_W = 1058$ K, both at 1 atm pressure, in Figure 21. The center temperature of the arc in eV is indicated on each plot as a parametric variable.

By choosing a channel size R, Figure 21 could be converted to characteristic curves, E vs J. Since we are most interested in the extinction field for a given channel size, we record the minimum $R \cdot E$ and note that this gives a model dependent constant for the product of channel size and extinction field. Converting to channel diameters we find:

	$D(cm) \cdot E_{ext}(V/cm)$
Hg (1) ; p = 1 atm; T_W = 629 K	3. 19 V
Hg (2) ; p = 1 atm; T_W = 629 K	3. 38 V
Hg (3) ; p = 1 atm; T_W = 629 K	3. 01 V
Hg (1) ; p = 1 atm; T_W = 2321 K	3. 11 V
Hg (1) ; p = 10 atm; T_W = 629 K	3. 30 V
NaK ; p = 1 atm; T_W = 1058 K	2. 05 V

Note that substantial changes in the electron-neutral cross section, ion-neutral cross section, wall temperature, and pressure produce minor changes in the result for Hg. The result is sensitive to the atom-atom cross section through the atomic contribution to heat conductivity, however. Note also that for the same channel NaK gives an extinction field significantly lower than Hg.

The Hg results are compared with Harris's earlier theory and some experimental data in Figure 17 where extinction field is plotted versus channel diameter. Harris's results are indicated as horizontal error bars and the data from earlier fuse tests (Figure 22) is summarized as curves for alumina and sapphire. Using the results of the above range of Hg models, the uncertainty in the present theory is indicated. The agreement of both theories and experiment is good.
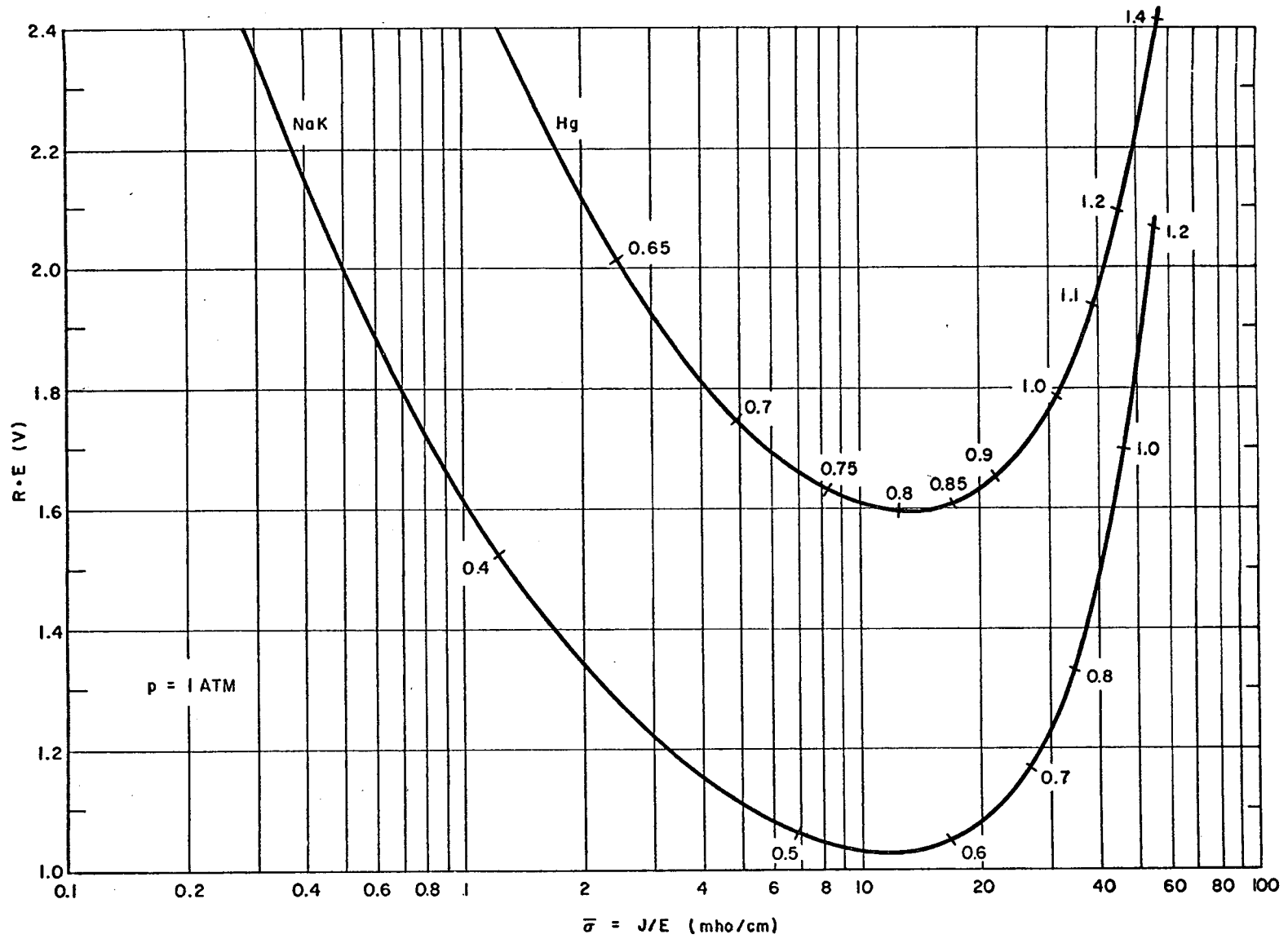
48

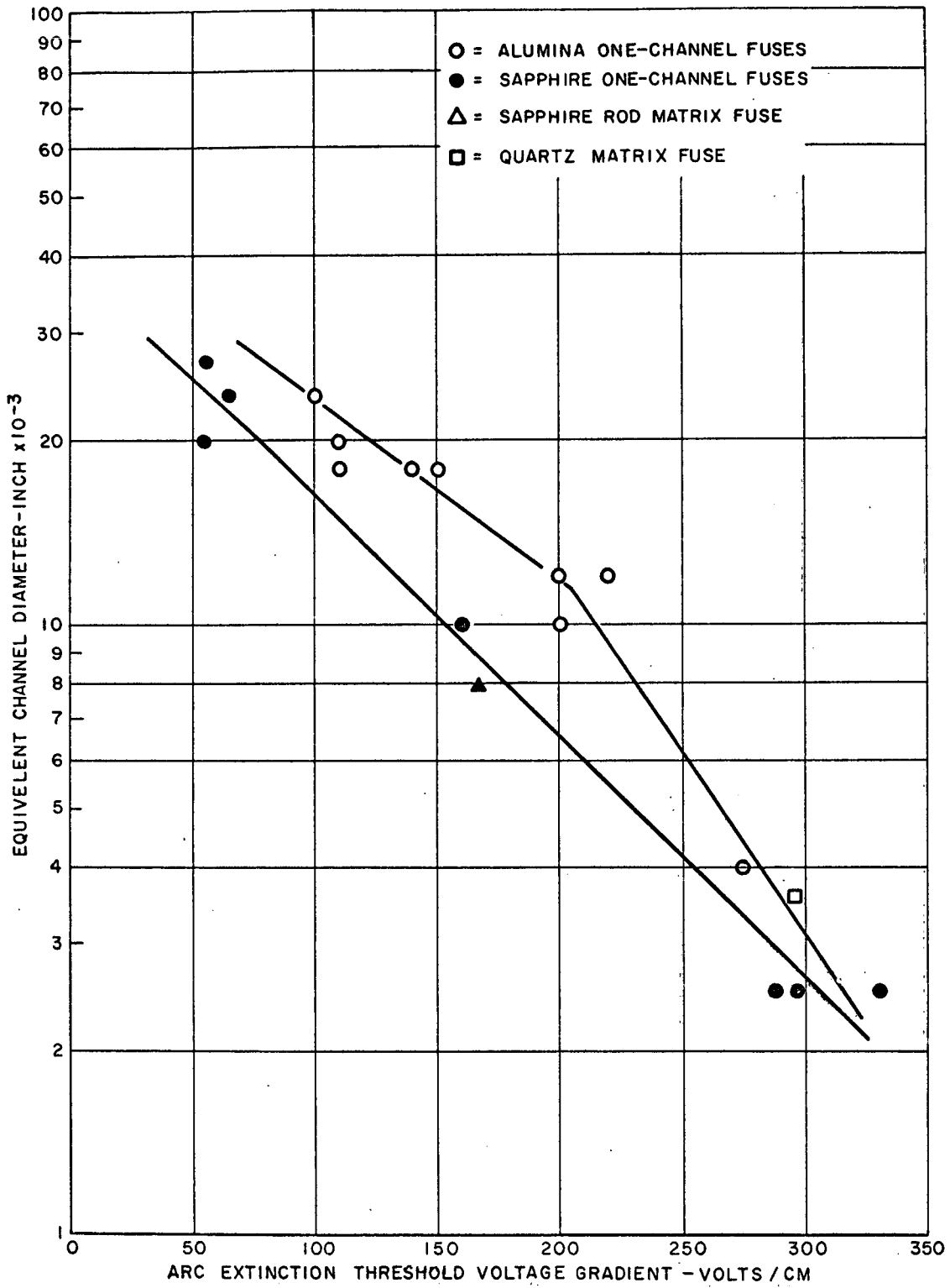Figure 21 - Results of Computer Program for Mercury and NaK Metal Vapor Arcs

Figure 22 - Arc Extinction Voltage Variations with
Channel Diameter

```
00010 COMMON T(2),D(2),P,RE,S,K
00020 DIMENSION TEMP(30)
00030 REAL K,KO,JIE
00040 FILENAME OF
00050 EXTERNAL DERIV
00060 NIT=0
00070 MT=0
00080 PRINT:"OUTPUT FILENAME":READ:OF
00090 10PRINT:" ":PRINT:" ":PRINT:"PRESSURE"
00100 READ:P
00110 IF(P.LE.0.)GO TO 999
00120 TW=0.05421/(1.-0.089*ALOG(P))
00130 PRINT 1000,TW
00140 1000FORMAT(" TW =",1PE9.2)
00150 30PRINT:" ":PRINT:" ":PRINT:"TO"
00160 READ:TO
00170 IF(TO.LE.0.)GO TO 10
00180 CALL TRANSP(P,TO,SO,KO)
00190 REO=SQRT(4.*KO*TO/SO)
00200 NP=2./REO+1.
00210 PRINT 1001,REO,NP
00220 1001FORMAT("+REO =",1PE9.2,I10," NP")
00230 READ:NP
00240 DRE=0.1/NP
00250 RE=0.
00260 T(1)=TO:T(2)=0.
00270 FIE=0.
00280 JIE=SO
00290 WRITE(OF,2000)P,TO,TW
00300 2000FORMAT(///"PRESSURE =",F8.3," ATM"/"CENTER TEMPERATURE =",
00310 &    1PE10.3," EV"/"WALL TEMPERATURE =",1PE10.3," EV"/
00320 &    5X,"RE(V)",5X,"T(EV)",1X,"K(W/CMEV)",1X,"S(MHO/CM)",
00330 &    1X,"J/E(MO/C)",1X,"F/E(A/CM)")
00340 WRITE(OF,2010)RE,T(1),KO,SO,JIE,FIE
00350 2010FORMAT(6(1PE10.2))
00360 IND=0:NRR=0
00370 100NRR=NRR+1
00380 CALL AMPB1(IND,DERIV,TEMP,RE,DRE,T,D,2,NR,NIT,MT)
00390 IF((1.+DRE*D(1)/T(1)).LT.0.8)IND=1
00400 CALL AMPB2(IND,DERIV,TEMP,RE,DRE,T,D,2,NR,NIT,MT)
00410 IF(S.GT.0.)GO TO 110
00420 RE=RE*EXP(10.932*(TW**2-T(1)**2)/T(2))
00430 T(1)=TW
00440 GO TO 300
00450 110IF((T(1)+T(2)*DRE/(RE*K)).GT.TW)GO TO 200
00460 RE=RE+RE*K*(TW-T(1))/T(2)
00470 T(1)=TW
00480 GO TO 300
00490 200IF(MOD(NRR,NP).NE.0)GO TO 100
00500 300JIE=-2.*T(2)/RE**2
00510 FIE=-T(2)/RE
00520 WRITE(OF,2010)RE,T(1),K,S,JIE,FIE
00530 IF(T(1).GT.TW)GO TO 100
00540 PRINT 1010,RE,JIE,FIE
00550 1010FORMAT("  RE =",F9.3," V"/" J/E =",1PE9.2," MHO/CM"/
00560 &    " F/E =",1PE9.2," AMP/CM")
00570 GO TO 30
00580 999STOP
00590 END
00600 SUBROUTINE DERIV
00610 COMMON T(2),D(2),P,RE,S,K
00620 REAL K
00630 CALL TRANSP(P,T(1),S,K)
00640 D(1)=0.
00650 IF(RE.GT.0.)D(1)=T(2)/(RE*K)
00660 D(2)=-RE*S
00670 RETURN
00680 END
```

SUBROUTINE FOR MERCURY

```
00010 SUBROUTINE TRANSP(P,T,S,K)
00020 REAL K,KE,KA,KR,N,NE,LAM
00030 A=2.
00040 QAA=(8.96E-16)/SQRT(T)
00050 QAI=1.E-14
00060 QIA=1.E-14
00070 QEAVE=(2.34E-7)*SQRT(T)
00080 V1=10.434
00090 S=0.;X=0.
00100 IF(T.LE.0.15)GO TO 10
00110 C=4.*4.773E3*EXP(-V1/T)*T**2.5/P
00120 X=SQRT(C/(1.+C))
00130 N=6.325E17*P/T
00140 NE=N*X/(1.+X)
00150 LAM=1.549E10*T**1.5/SQRT(2.*NE)
00160 SEI=1.915E2*T**1.5/ALOG(LAM)
00170 SEN=(2.818E-4)*X/(QEAVE*(1.-X))
00175 F=1.-0.2/(1.+(0.4343*ALOG(1.2*SEN/SEI))**2)
00180 S=F*SEI*SEN/(SEI+SEN)
00190 10KE=A*T*S
00200 KA=(1.959E-14)*SQRT(T)*(1.-X)/((1.-X)*QAA+X*QAI)
00210 KR=0.
00220 FR=V1/T+2.5-0.5/(1.-X)
00230 IF(FR.GT.0.)KR=(7.386E-15)*SQRT(T)*X*(1.-X)*FR**2/QIA
00240 K=KE+KA+KR
00250 RETURN
00260 END
```

SUBROUTINE FOR NaK

```
00010 SUBROUTINE TRANSP(P,T,S,K)
00020 REAL K,KE,KK,KNA,N,NE,LAM
00030 EPS=0.0005
00040 A=2.
00050 QEKVE=1.6E-6
00060 QENAVE=1.2E-6
00070 QKK=5.47E-15
00080 QNANA=3.30E-15
00090 QNAK=4.32E-15
00100 QKIK=2.E-14
00110 QNAINA=1.5E-14
00120 VK=4.339;VNA=5.138
00130 XK=0.;XKN=0.;XNA=0.;XNAN=0.
00140 S=0.
00150 IF(T.LE.0.1)GO TO 10
00160 CK=4.773E3*EXP(-VK/T)*T**2.5/P
00170 CNA=4.773E3*EXP(-VNA/T)*T**2.5/P
00180 20XKN=(SQRT(8.*CK*(3.+XNA)*(1.+CK)+(CK+XNA*(1.+CK))**2)
00190 &   -CK-XNA*(1.+CK))/(4.*(1.+CK))
00200 XNAN=(SQRT(4.*CNA*(3.+2.*XKN)*(1.+CNA)+(2.*CNA+2.*XKN*
00210 &   (1.+CNA))**2)-2.*CNA-2.*XKN*(1.+CNA))/(2.*(1.+CNA))
00220 IF((ABS(XKN-XK).LE.(EPS*XK)).AND.(ABS(XNAN-XNA).LE.(EPS*XNA)))
00230 &   GO TO   30
00240 XK=XKN;XNA=XNAN
00250 GO TO 20
00260 30XK=XKN;XNA=XNAN
00270 N=6.325E17*P/T
00280 NE=N*(XK+0.5*XNA)/(1.5+XK+0.5*XNA)
00290 LAM=1.549E10*T**1.5/SQRT(2.*NE)
00300 SEI=1.915E2*T**1.5/ALOG(LAM)
00310 SEK=(2.818E-4)*(XK+0.5*XNA)/(QEKVE*(1.-XK))
00320 SENA=(2.818E-4)*(XK+0.5*XNA)/(QENAVE*0.5*(1.-XNA))
00330 SEN=SENA*SEK/(SENA+SEK)
00340 F=1.-0.09/(1.+(0.4343*ALOG(1.1*SEN/SEI))**2)
00350 S=F*SEI*SEN/(SEI+SEN)
00360 10KE=A*T*S
00370 KK=(5.021E-14)*SQRT(T)*(1.-XK)/(1.13137*(1.-XK)*QKK
00380 &   +1.13137*XK*QKIK+1.1868*0.5*QNAK)
00390 KNA=(6.548E-14)*SQRT(T)*(1.-XNA)/(1.13137*(1.-XNA)*QNANA
00400 &   +1.13137*XNA*QNAINA+1.1062*2.*QNAK)
00410 K=KE+KK+KNA
00420 RETURN
00430 END
```

APPENDIX B

EVALUATION OF THE RADIATION
COOLING MECHANISM OF MERCURY VAPOR ARCS

Dr. L. P. Harris

Although radiation cooling had appeared to be an important factor in the energy exchange processes of mercury arcs based on earlier calculations some improved calculations indicate that radiation cooling is not a strong factor for arcs experienced in this program. (Refer to Report CR-72868, p. 81). For a discharge at the blackbody limit ($\epsilon_r = 1$),

$$E\sqrt{t} = \left(2 \frac{ST_o^4}{\sigma_o}\right)^{1/2}$$

The discharge current is then determined by

$$J\sqrt{t} = \sigma_o \left(E\sqrt{t}\right)$$

In these equations E and J are the voltage gradient and current density, t is the discharge thickness (slab arc) or radius (cylindrical arc), S is the Stefan-Boltzmann constant, T_o the discharge temperature, and σ_o the plasma conductivity.

Figure 23 shows a comparison with experimental data of the $E\sqrt{t}$ vs $J\sqrt{t}$ characteristic calculated from the preceding equations for mercury. The experiments were done about 1964 with cylindrical discharges of 0.5 to 1.5 millimeter diameter. For values of $J\sqrt{t}$ below about 2×10^3 A/cm$^{3/2}$ the blackbody calculation gives too high a voltage gradient and power dissipation, but for $J\sqrt{t} > 2 \times 10^3$ A/cm$^{3/2}$ the experimental points appear to follow the theoretical curve. Thus it appears that mercury arcs over 70 amperes in a 1.0 mm diameter channel or over 25 amperes in 0.5 mm diameter might be cooled by blackbody radiation.
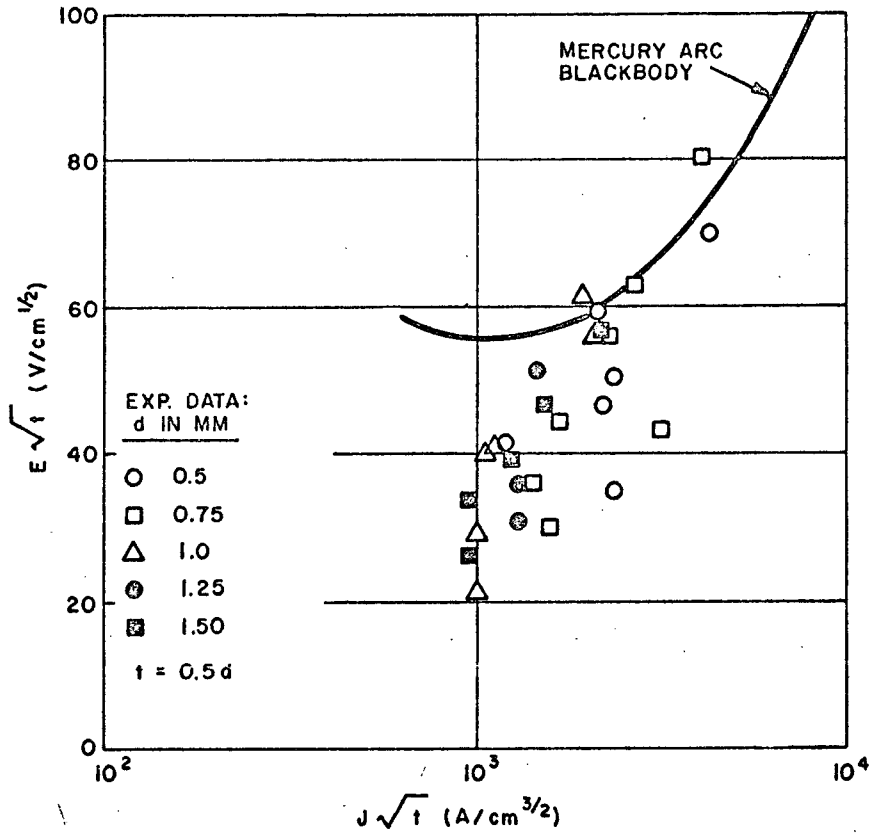
Figure 23 - Comparison of Mercury Arc Blackbody
Analysis with Experimental Data

THE FOLLOWING PAGES ARE DUPLICATES OF

ILLUSTRATIONS APPEARING ELSEWHERE IN THIS

REPORT.   THEY HAVE BEEN REPRODUCED HERE BY

A DIFFERENT METHOD TO PROVIDE BETTER DETAIL